

Document-34898
Bo Xin
Doug Neil
Sandrine Thomas
For the LSST M1M3 Team
April 14, 2020

M1M3 Optical Testing Results at the UofA Mirror Lab

Abstract

The M1M3 optical testing at the University of Arizona (UofA) Richard F. Caris Mirror Lab has been very successful. This document describes the analysis results from those testing campaigns.

Contents

1	Introduction	2
2	Coordinate System Definition	4
3	Optimize Measurement Parameters	5
3.1	Number of samples and time interval for each measurement	5
3.2	Number of measurements for averaging	7
4	Repeatability Tests	7
4.1	Add low-order bending mode, then remove it	8
4.2	Add high-order bending mode, then remove it	9
4.3	Translate the mirror, then back	9
4.4	Lower the mirror, then raise it	10
4.5	Remove an actuator, then reinstall it	10

5	Bending modes	11
5.1	FEA bending modes	12
5.2	Measured bending modes	14
5.3	Bending Modes Scaling Factors and Cross-Talks	16
5.4	Final Bending Modes	19
6	Single actuator influence functions	20
7	Surface optimization	23
7.1	Initial force calculation	24
7.2	Divits above the quads	24
7.3	Final Optimized Surfaces and Forces	28
7.4	M1M3 Structure function	29
7.5	Image Quality Evaluation	30
7.6	Use of bending mode No. 27	30
7.7	Building the LUT	32
8	Horizon tests	35
8.1	Horizon Bending Test	35
8.2	Inferring M1 shape from M3 measurements	37
9	Actuator Force Error	38
10	Performance of the EFD	40
11	Summary	40

1 Introduction

In January and February 2019, the fully assembled M1M3 system, with the glass mirror on top of the mirror cell, modulo the thermal control system, underwent actuated test at the UofA Mirror Lab. The testing consisted of two testing campaigns, each lasted approximately two weeks. First campaign from 1/14 to 1/25, minus Monday 1/21 which was MLK day. The second from 2/11 to 2/22, minus Friday 2/22 which was Rodeo day. In this document, we describe the analysis results from those testing campaigns.

The main objectives of the testing campaigns were two-fold: (1) optimizing the M1M3 surface, with optimized support forces, and (2) characterizing how the surface responds to actuator forces, including measuring the bending modes and single actuator influence functions.

Both main objectives were successfully achieved. Of course, during the process, we exercised the control software, and the hardware, learned a lot about the as-built system, and came up with a long list of items that could be further improved, as summarized by Doug Neil in his lessons-learned document. But those are not the major topic for this document. We will just say that the entire software plus hardware system have been very robust. They worked for the entire testing campaigns, without any glitches, and without being powered down. The only exception is the Engineering Facility Database (EFD), which we will discuss in my detail in Section 10. Everything has been very repeatable, as we will see from some analysis results we will present later in this document.

The analysis has been done in Python notebooks, and documented on GitHub https://github.com/lsst-sitcom/M1M3_ML. The only exception is that some of the real-time analysis, where fast turn-around was needed, was done in Matlab. This is because most of the analysis done at the M1M3 acceptance, described in document-17171 [1], was done in Matlab. The notebooks provide both a day-by-day accounting of what was done, i.e., what results were obtained on each day, why we did what we did, and some more targeted analysis, including tutorials. Other than holidays, there is no notebook for 1/23 because on that day the Mirror Lab crew performed CGH calibration and worked on empirical force analysis for fixing the divits above the quads. A summary of what tests have been performed for each of the major tasks can be found in `summary_by_task.txt` in the GitHub repo.

Other useful background information relevant to the testing include

- UofA test plan [2]
- Data analysis plan presented at M1M3 Optical Test Readiness Review [3]
- Data processing procedure description [4]
- M1M3 performance analysis at mirror acceptance (2015) [1].

Note that the Mirror Lab also produced a data analysis report for these testing campaigns [5]. What we describe here in this document is complimentary to the Mirror Lab report. We do not want to duplicate work. It should be noted that in a lot of cases, where we have examined the Mirror Lab data processing and analysis in detail, and felt that we understand everything, we simply use their results, or refer to figures and tables in their report directly. As one can see from the Python notebooks, in those cases, we simply read the Mirror Lab analysis output from the data packages they provided.

In the rest of this document (Sections 3 through 8), we will describe each major task in a separate section. We follow the order as outlined in `summary_by_task.txt` in the above GitHub repo. Section 9, the actuator force error analysis, was not a major task as listed in the test plan. But with all the data we collected it came for free. It should be noted that the order the tasks and results are described in this document does not reflect the order the tests were carried out during the testing. The order the tests were executed in the Mirror Lab had to take into account practicality, to make sure things run smoothly and efficiently.

Note that most of the measurements we took were differential measurements, i.e., we were more interested in the differences between subsequent measurements, rather than individual

measurements. Measurements were always taken as quickly as possible, to avoid thermal drifts, which could invalidate differential measurements. Thermal corrections are not included in most of the data processing.

2 Coordinate System Definition

Before doing any quantitative analysis, it is important to make sure we have a clear definition of the coordinate system. Figure 1 shows the layout of the 156 actuators, as in the M1M3 optical coordinate system. This is looking at the M1M3 surface from M2. This will be the standard coordinate system we use for all the analysis presented in this document. The mirror cell access door is at the $+y$ position. In the Mirror Lab, the x -axis pointed toward the control station.

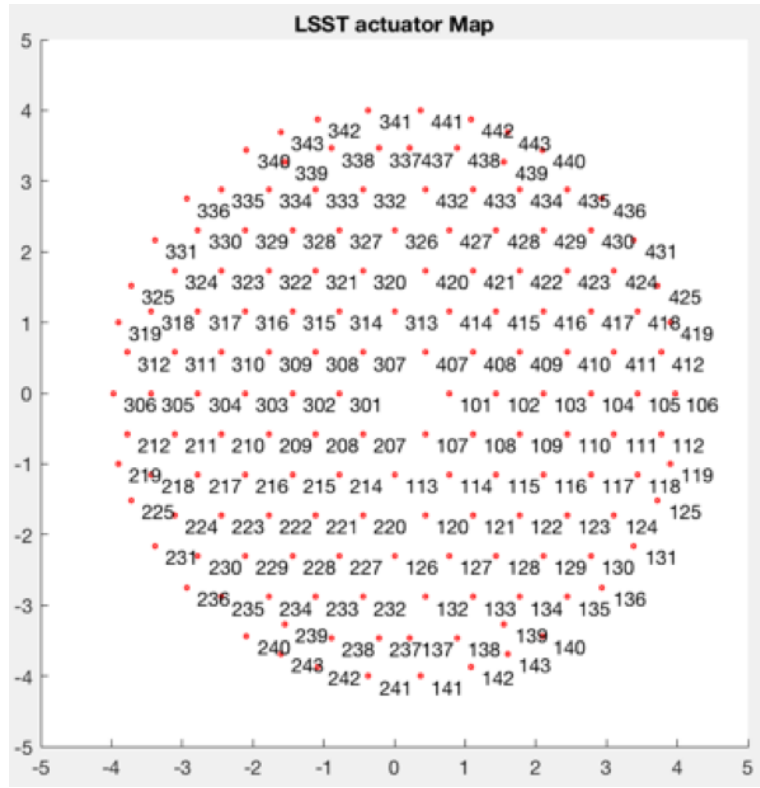


Figure 1: M1M3 actuator ID numbers in the M1M3 optical coordinate system. This is looking at the M1M3 surface from M2. This will be the standard coordinate system we use for all the analysis presented in this document.

We note that most of the LSST engineering drawings use a different coordinate system, as shown in Figure 2. The y axis is the same as the M1M3 optical coordinate system, but the x axis is flipped. The mirror cell access door is still at the $+y$ position. In the Mirror Lab, the x -axis pointed away from the control station. This is more intuitive when one works inside the mirror cell, for example, while installing the actuators.

Figure 2 also shows the actuator ID numbers and their types. The actuator types indicate whether it is a single-axis actuator (SAA) or dual-axis actuator (DAA), the orientation of the secondary cylinder, which is also indicated by the arrows in Figure. 2, and the number of pucks for each load-spreader. The index keys can be found in https://github.com/lsst-sitcom/M1M3_ML/blob/master/data/LS_CUP_ACTSTYLE_ID.xlsx.

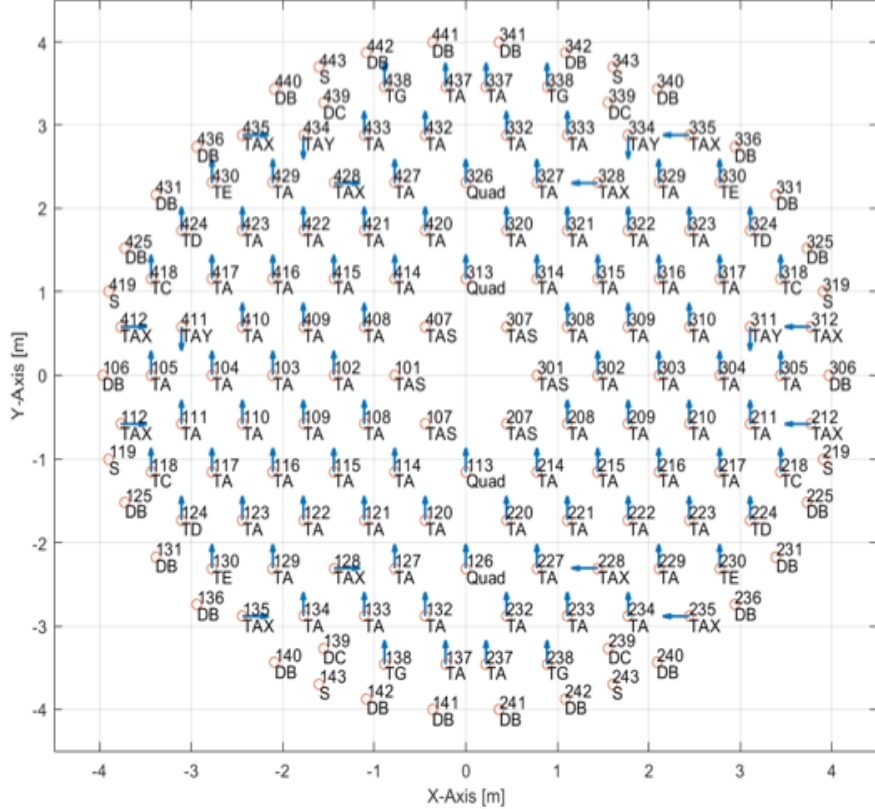


Figure 2: M1M3 actuator ID numbers, types, and their locations while looking at the mirror from inside the cell.

Before any tests began, we verified with the Mirror Lab that we were using the same coordinate system, and the x and y coordinates of the actuators all agree.

3 Optimize Measurement Parameters

3.1 Number of samples and time interval for each measurement

Due to instabilities in the testing hardware, mostly from air turbulence in the optical path and hardware vibration, each surface measurement is an average of many samples. A sample itself is the average of a series of short exposures, where the averaging is done automatically by the 4D software that came with the interferometer. The number of samples for each surface measurement, and the time interval between the samples, are configurable parameters. We use

the shorthand $a \times bs$ for a samples separated by b seconds. Before we start taking measurements to characterize the mirror bending properties and optimizing the mirror surfaces, we need to optimize a and b .

To determine a and b , we tested three configurations, each taking an equal amount of time to acquire:

1. $10 \times 5\text{s}$
2. $5 \times 10\text{s}$
3. $25 \times 2\text{s}$

We did this for M1 only. For each configuration, we took 4 measurements. For each measurement, we take the average of all the samples, s_1, s_2, s_3, s_4 (we call these sub-averages), then average the 4 measurements, $s = (s_1 + s_2 + s_3 + s_4)/4$. The sub-averages for the $25 \times 2\text{s}$ configuration is shown in Figure 3.

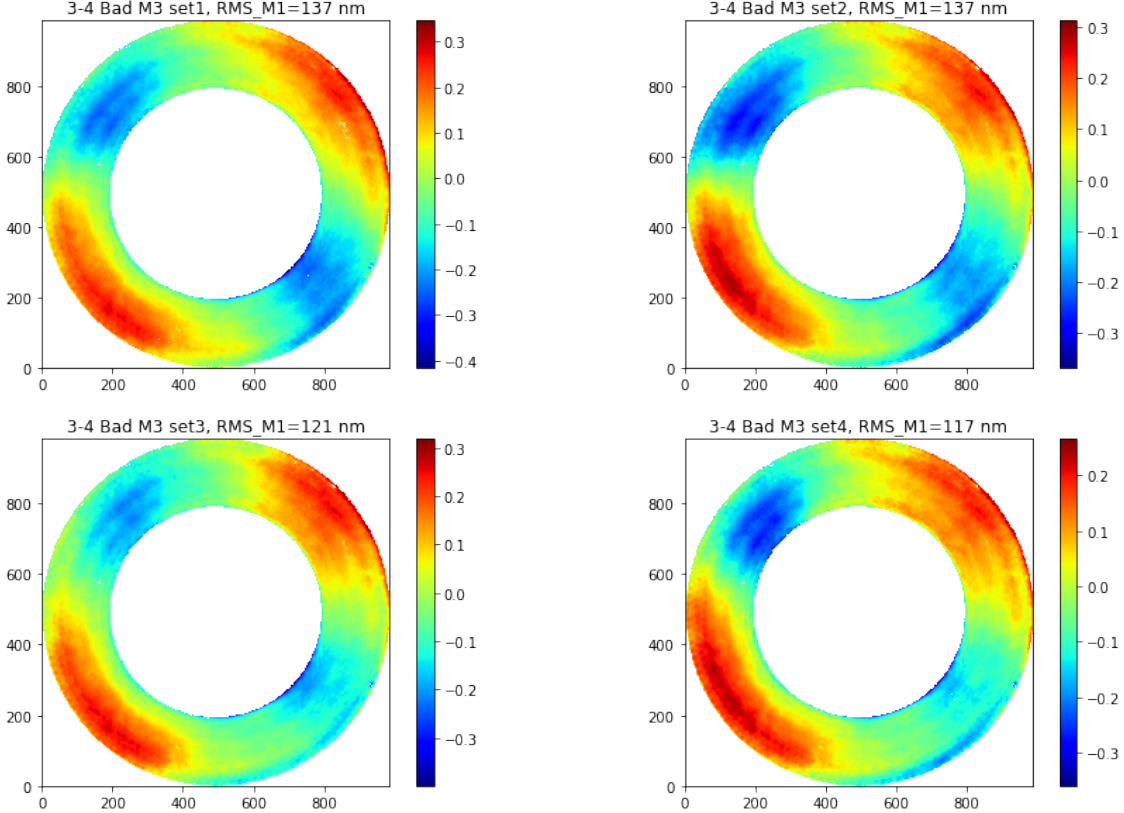


Figure 3: M1 surface maps sub-averages with the $25 \times 2\text{s}$ configuration.

The RMS of the difference maps between these sub-averages shown in Figure 3 and their grand-average (s) is calculated to be 24 nm. For comparison, the same RMS values for the $10 \times 5\text{s}$ and $5 \times 10\text{s}$ configurations are found to be 28 nm. As another check, we also repeated

this test with a $40 \times 5\text{s}$ configuration. With much longer averaging time, the RMS difference between the sub-averages and the grand-average remained at 24 nm. We therefore concluded that the $25 \times 2\text{s}$ configuration is very close to optimal, and decided to use that for all subsequent measurements.

The analysis in Jupyter Notebook format is found at https://github.com/lsst-sitcom/M1M3_ML/blob/master/190115.ipynb

3.2 Number of measurements for averaging

To determine the number of measurements needed for averaging, we took 10 M1 measurements, then 20 M3 measurements, then another 10 M1 measurements. For the analysis part, we subdivide these 20 M1 and 20 M3 measurement into groups of 2, 5, and 10 measurements. Within each group, we calculated the group sub-averages, and the grand-average of all the measurements. The idea is that the grand-averages can be used as the “truth”, and we calculate the RMS differences between the sub-averages and the grand-averages. Note that the average of the first 10 M1 measurements was seen to be very different from the second 10 M1 measurements, so we had to use 2 grand-averages for M1.

The criteria was that we want the noise on the surface measurements in RMS to be less than 20 nm. This corresponds to the non-repeatable error in the surface measurements. With the initial acceptance testing, we got the RMS error on both surfaces below 20 nm. Note that the as-built M1M3 surface, as measured during M1M3 acceptance testing, contributes to 120 mas in PSF FWHM, including 104 mas from M1 and 60 mas from M3 [1]. The total error budget allocated to the as-built LSST system is 400 mas.

We refer the reader to Figures 1 and 2 of the Mirror Lab analysis report [5] for the RMS differences versus the number of measurements in groups. As can be seen there, for M3, things converge pretty quickly. We only need one measurement for M3. We could even shorten each M3 measurement to be $20 \times 2\text{s}$ without sacrificing much measurement accuracy. For M1, 2 measurements, each of $25 \times 2\text{s}$, would be needed. So from this point on, we define each M1 measurement as $50 \times 2\text{s}$, and each M3 measurement as $20 \times 2\text{s}$. As the result, for the bending modes and influence function measurements, M1 took much longer than M3.

We want the measurements to be long enough to average out the fast-changing factors, such as the air turbulence. Meanwhile we do not want an individual measurement to take too long, because thermal conditions would be slowly drifting.

The analysis in Jupyter Notebook format is found at https://github.com/lsst-sitcom/M1M3_ML/blob/master/190115.ipynb

4 Repeatability Tests

We did a lot of repeatability tests, which we discuss in detail next. This involved adding additional forces to the actuators to produce a low-order or high-order bending mode, then removing it, or translating the mirror using the hard points then translating back, etc. At the

end of the operations, we remeasure the mirror surfaces, and see how much has changed in surface measurements.

We assumed that M1 is more sensitive to perturbations, due to its larger diameter. For most of these repeatability tests, we measured M1 only. For the test where we removed an actuator then reinstalled it, we measured both M1 and M3, as some actuators removed were under M3.

Right before these tests, we measured the reference surfaces , which is shown in Figure 4. The reference forces were one of the force sets obtained during the early optimization process. It doesn't matter what exact forces we use, as long as they give a good measurable surface. We are only interested in the differences between measurements.

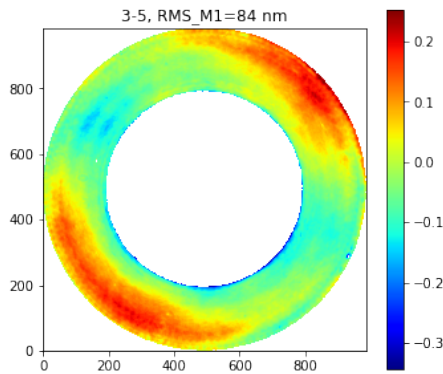


Figure 4: M1 reference surface before the repeatability tests.

Most of the analysis described in this section is found at https://github.com/lsst-sitcom/M1M3_ML/blob/master/190116.ipynb. The only exception is that the removing and reinstalling actuator part is in https://github.com/lsst-sitcom/M1M3_ML/blob/master/190221.ipynb

4.1 Add low-order bending mode, then remove it

For low order bending modes, a small amount of forces produce a relatively large surface deformation, measured by the surface RMS. When applying bending modes to introduce surface deformations during the testing, based on the Mirror Lab experience, a general rule of thumb is that a surface RMS of about 500 nm or below is desirable. This is large enough for it to be seen by the interferometer, but not too large to cause confusion in interpreting the fringes.

Based on the 500 nm rule, we applied 3N of RMS forces to produce bending mode No. 1, which is one of the two astigmatism modes, then removed it, then remeasured the M1 surface. Figure. 5 shows the new map, as well as the difference from the reference map. The RMS of the difference map is 20 nm, which is on the same level as the measurement accuracy.

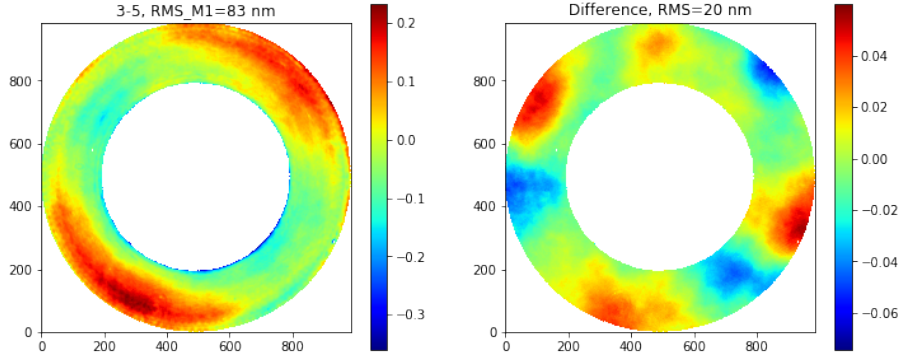


Figure 5: Measured M1 surface after we added 3N of bending mode No. 1 then removed it (left), and the difference from the reference map (right). The reference map is shown in Figure. 4.

4.2 Add high-order bending mode, then remove it

Repeating the procedure as described in Section. 4.1 with a high order bending mode, 20N RMS of No. 22 in this case, gave us results shown in Figure. 6. The RMS of the difference map is 17 nm, which is on the same level as the measurement accuracy.

Repeating the procedure with 40N and 60N RMS of bending mode No. 22 gave very similar results. The RMS of the resulting difference maps were 14 nm and 18 nm, respectively, in those two cases.

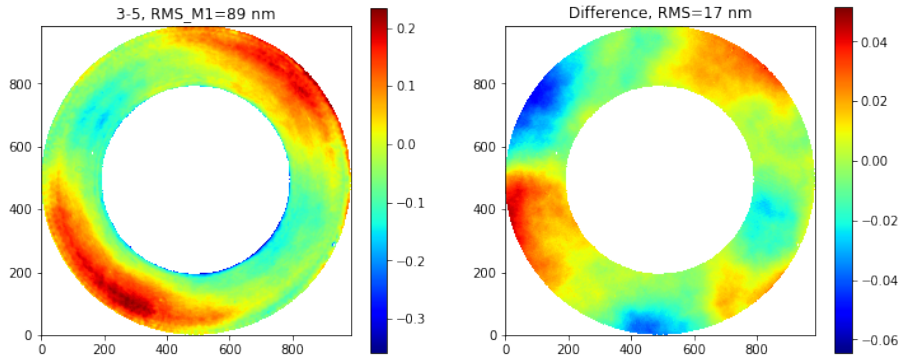


Figure 6: Measured M1 surface after we added 20N of bending mode No. 22 then removed it (left), and the difference from the reference map (right). The reference map is shown in Figure. 5 (left).

4.3 Translate the mirror, then back

Next, we repositioned the mirror using the hard points, specifically, by translating the mirror 1 mm along $+x$ axis, then translate it back, and remeasure the M1 surface. We also repeated

this procedure for $+y$ and $+z$ directions. As the example, results for $+x$ translation is given in Figure. 7. The resulting RMS of the difference maps are 17, 17, and 33 nm, for the x, y, and z translations, respectively.

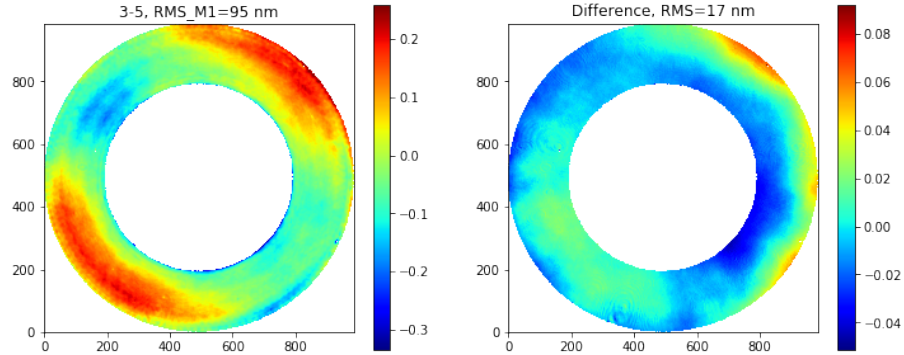


Figure 7: Measured M1 surface after we translated the mirror along $+x$ direction by 1mm, then moved it back (left), and the difference from the reference map (right). The reference map here is the M1 map after we removed the 60 N RMS of bending mode No. 22.

4.4 Lower the mirror, then raise it

We then lowered the mirror onto its static supports, then raised it, reapplied the nominal forces, then remeasured M1 surface. The observed RMS difference was 39 nm, as shown in Figure 8.

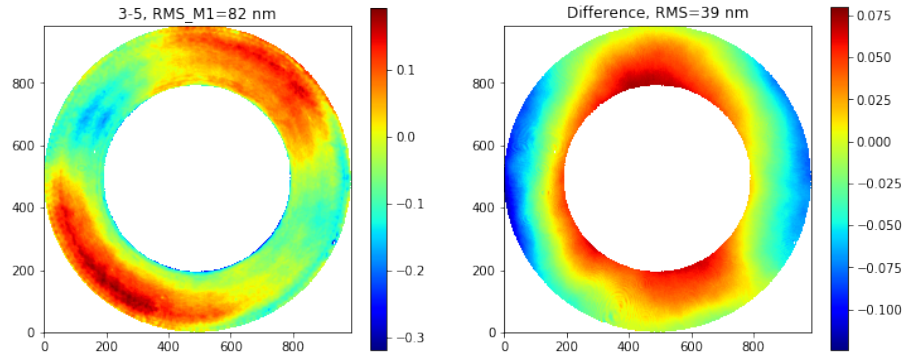


Figure 8: Measured M1 surface after we lowered, then raised the mirror (left), and the difference from the reference map (right). The reference map is the M1 map after we moved the mirror back to nominal position after the 1 mm $+z$ translation.

4.5 Remove an actuator, then reinstall it

Because the mirror would need to be detached from the cell before the two being shipped to Chile separately, we wanted to understand better how repeatable the actuator installations are.

To do this test, we picked four actuators, with ID numbers 337, 114, 113, 411, representing different actuator types and various locations. We removed and re-installed each actuator one after another, and measured surfaces in between this process. For example, we first take a M1-M3-M1 reference measurement, then removed actuator 337, followed by a reinstallation of actuator 337. Then we take the second M1-M3-M3 measurement.

There were a total of five surface measurements, before and after removing and reinstalling the four actuators. The five surface measurements are shown in Figure 9. The four difference maps are shown in Figure 10. The RMS values of all the surface measurements as well as the different maps are shown on plot titles.

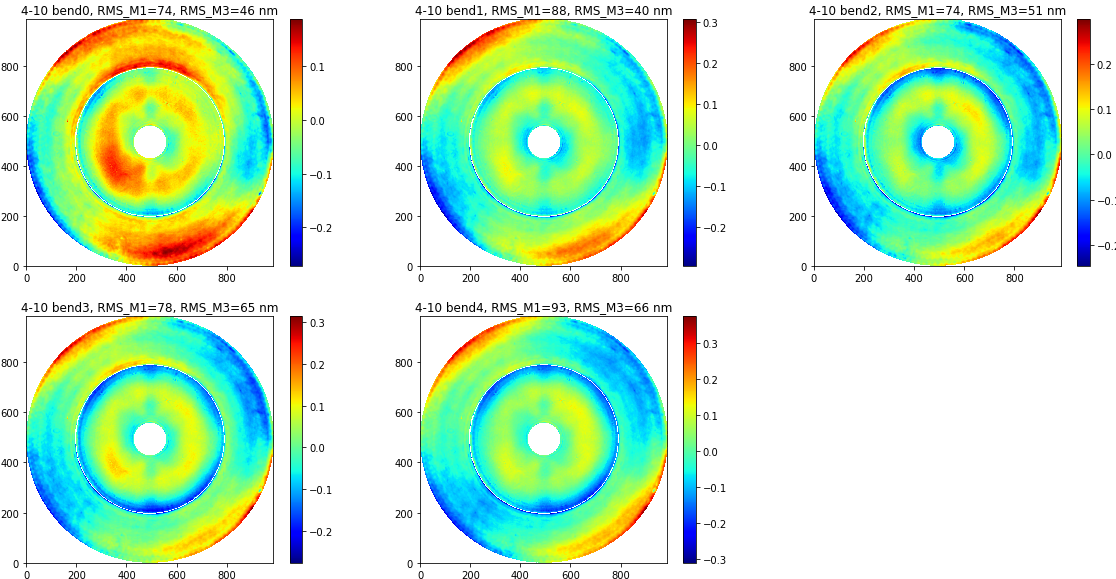


Figure 9: M1 and M3 surface maps before and after removing and reinstalling the four actuators.

The RMS values of these difference maps are somewhat larger than the 20 nm measurement accuracy, but not much larger. On the other hand, these difference maps seem to have structures that are not consistent with being completely random. We believe that this is due to technicians thermally disturbing the environment inside the cell while removing and installing the actuators.

5 Bending modes

One of the major objectives of the Mirror Lab testing was to calibrate the FEA-derived bending modes.

In this section, we first explain how we calculated the FEA bending modes. The actual bending mode measurements took place on 1/16, 1/17, and 2/11 for the Mirror Lab bending modes, and 2/13, 2/18, 2/19 for the LSST bending modes. The corresponding Jupyter Notebooks are

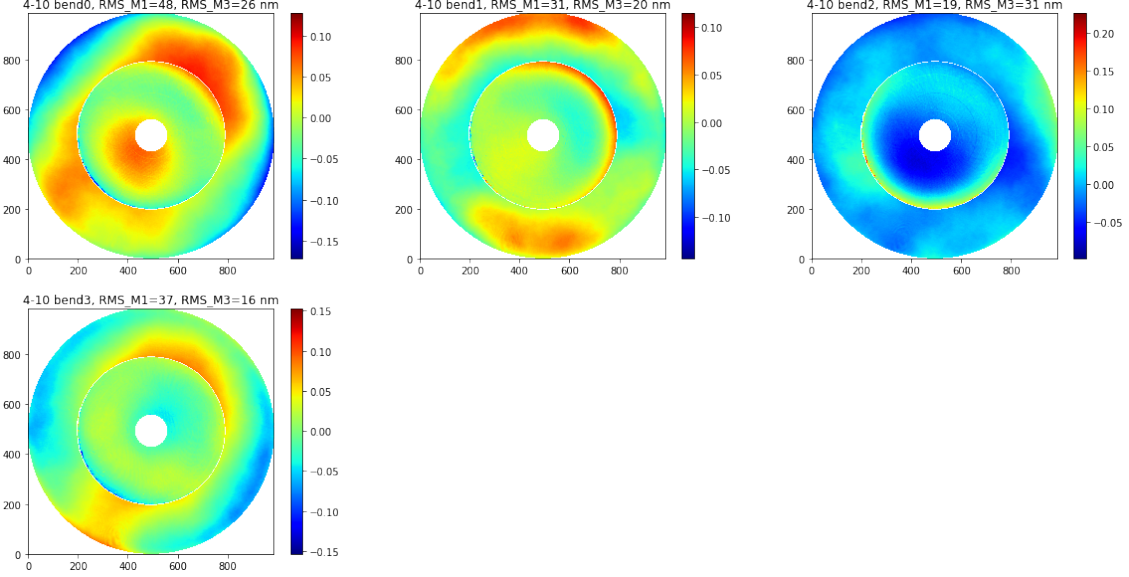


Figure 10: M1 and M3 surface difference maps between before and after reinstalling each actuator.

- https://github.com/lsst-sitcom/M1M3_ML/blob/master/190116.ipynb
- https://github.com/lsst-sitcom/M1M3_ML/blob/master/190117.ipynb
- https://github.com/lsst-sitcom/M1M3_ML/blob/master/190211.ipynb
- https://github.com/lsst-sitcom/M1M3_ML/blob/master/190213.ipynb
- https://github.com/lsst-sitcom/M1M3_ML/blob/master/190218.ipynb
- https://github.com/lsst-sitcom/M1M3_ML/blob/master/190219.ipynb

5.1 FEA bending modes

FEA bending modes calculation procedure is given in document-15312 [6]. Calculating the FEA bending modes is actually a non-trivial process. It is important to make sure we get the most accurate results from the FE model, because that is what we start with during the testing.

As a quick summary, it involves the following steps.

1. Deriving the unit-load force vectors. Each unit-load force vector has one actuator that pushes with a 1000 N force, while all other actuators work together to offset the net z -force and the x and y moments. In solving for 155 forces under 3 constraints, we assume the 155 forces have a 2D linear distribution, therefore only 3 coefficients are needed to determine all 155 forces. These 156 vectors, each has 156 elements, gives a matrix C , which is 156×156 .

2. Applying the unit-load force vectors to the FEA model of the mirror, and outputing the resulting surface shapes. For our FEA model we have 5256 surface nodes, therefore each surface shape is a 5256×1 vector, and we have 156 of these vectors. These 156 vectors, each 5256 elements long, gives a matrix D , which is 5256×156 .
3. Calculcating mirror influence matrix G . Because $D = GC$, so we have $G = DC^{-1}$.
4. Performing a singlar-value-decomposition (SVD) analysis of G , the output of which being all the bending modes and their corresponding force vectors. Since $G = U\Sigma V^T$, and U and V are unitary matrices, and we want to have bending modes with fixed surface RMS, e.g., RMS = 1 μm , we scale V to absorb Σ . Let V' be the bending mode force vectors, we can decompose any surface into $U\alpha$ and the corresponding force vector into $V'\alpha$.

$$U\alpha = (U\Sigma V^T)V'\alpha \quad (1)$$

Therefore

$$V' = V\Sigma^{-1} \quad (2)$$

There are a few subtle decisions to make, once we start to think about the details.

1. 156 forces versus 256 forces. In principle, the above procedure can be applied to all 256 actuators, treating each cylinder, or equivalently, F_y and F_z , as an independent actuator. Mathematically, this should give better results, because the lateral actuators can influence the mirror surface in z as well. But, in reality, these two different methods make very little difference in results, and it is much cleaner to only use the z forces to control mirror shape, y forces to offload gravity when we point off-zenith, and x forces for slewing and countering dynamics.
2. Subtraction of piston-tip-tilt (PTT) components from the unit-load surface shapes. In principle these should not be subtracted, because FE analysis verifies that even when the hard points are constrained, the surface shape can still have PTT, as the mirror is not a rigid body. So PTT will be part of what we put on the mirror surface when we command those bending mode forces. But, in reality, the amount of adjustments these PTT components requires from the hexapods is less than the hexapod motion resolution. Also note that we subtract PTT separately from M1 and M3 unit-load shapes, because the two interferometers are independent during the testing.
3. Surface sag, surface normal, versus z -displacements. For the purpose of testing the bending modes, we always use surface normal, because of the way interferometers work. The calibrated bending modes will also be in surface normal. But it is noted that when these bending modes are implemented in raytrace programs, they need to be projected to be surface sag, if that is how the distorted surfaces are defined. See Document-16390 [7] for the difference between the three.

We note that the Mirror Lab and LSST have maintained seperate FE models of the M1M3 mirror. We also calculated the bending modes separately. Before the testing started, we confirmed with each other we have been following the same calculation procedure the best we

know it. However, due to differences in the FE models, and the sensitivity of the bending modes calculation to numerical effects, the two sets of bending modes are a bit different.

For the bending mode measurements, which we will talk about next, we started with the Mirror Lab bending modes. However, as time went on, it appeared that the LSST bending modes are more effective when used for surface optimization. In this document, we will mostly focus on the measured LSST bending modes.

The bending modes derived by the LSST team from the LSST FE model is shown in Figure 11. Here we show the first 30 modes. The Active Optics System (AOS) baseline currently uses 20 modes. Considering numerical effects in the process of deriving FEA bending modes, the ordering of the modes could be a bit uncertain. At the beginning of the testing campaigns, the intention was to measure the first 22 bending modes. Later on during the surface optimization process, it was determined that bending mode No. 27 was needed for optimizing the mirror surface. We therefore measured modes 1-27. This will be discussed in detail later in Section 5.3.

5.2 Measured bending modes

To measure a bending mode B_i , we take the FEA-predicted forces for the mode F_i , apply them, then measure the change in the surface shape. The base force set F_0 , just like the one used in the repeatability test, is from one of the preliminary surface optimizations. It is a differential measurement, so details in F_0 doesn't matter much.

To further remove possible thermal drifts during the process, and to lower the error on the measurements, we always followed the following procedure:

1. apply $F_0 + F_i$, measure mirror surface to get S_{+1} ;
2. apply $F_0 - F_i$, measure mirror surface twice to get S_{-1} and S_{-2} ;
3. apply $F_0 + F_i$, measure mirror surface to get S_{+2} ;

We call this a $+ - - +$ measurement. In reality, we want these forces to produce surfaces with RMS of roughly 500 nm, so that the surface measurements would be of good accuracy. So most of the time the actual F_i is a scaled version of the FEA determined force set F_i^{FEA} . The actual RMS values for each bending mode, for M1 and M3 separately, are listed in Table 5 of the Mirror Lab analysis document [5], therefore not repeated here.

Because measuring M1 surface requires stowing the M3 bridge, instead of finishing both M1 and M3 surface measurements for a bending mode then moving onto the next bending mode, we always did the above for many M1 modes before moving onto the same set of M3 modes.

The measured bending mode (for M1 or M3) is

$$B_i = \frac{S_{+1} + S_{+2} - S_{-1} - S_{-2}}{2} \times \frac{RMS(F_i^{FEA})}{RMS(F_i)}. \quad (3)$$

As examples, Figure 12 shows the $+ - - +$ measurements for M1 bending modes No. 17, 18, and 20. The resulting measured bending modes, for both M1 and M3, are shown in Figure 13.

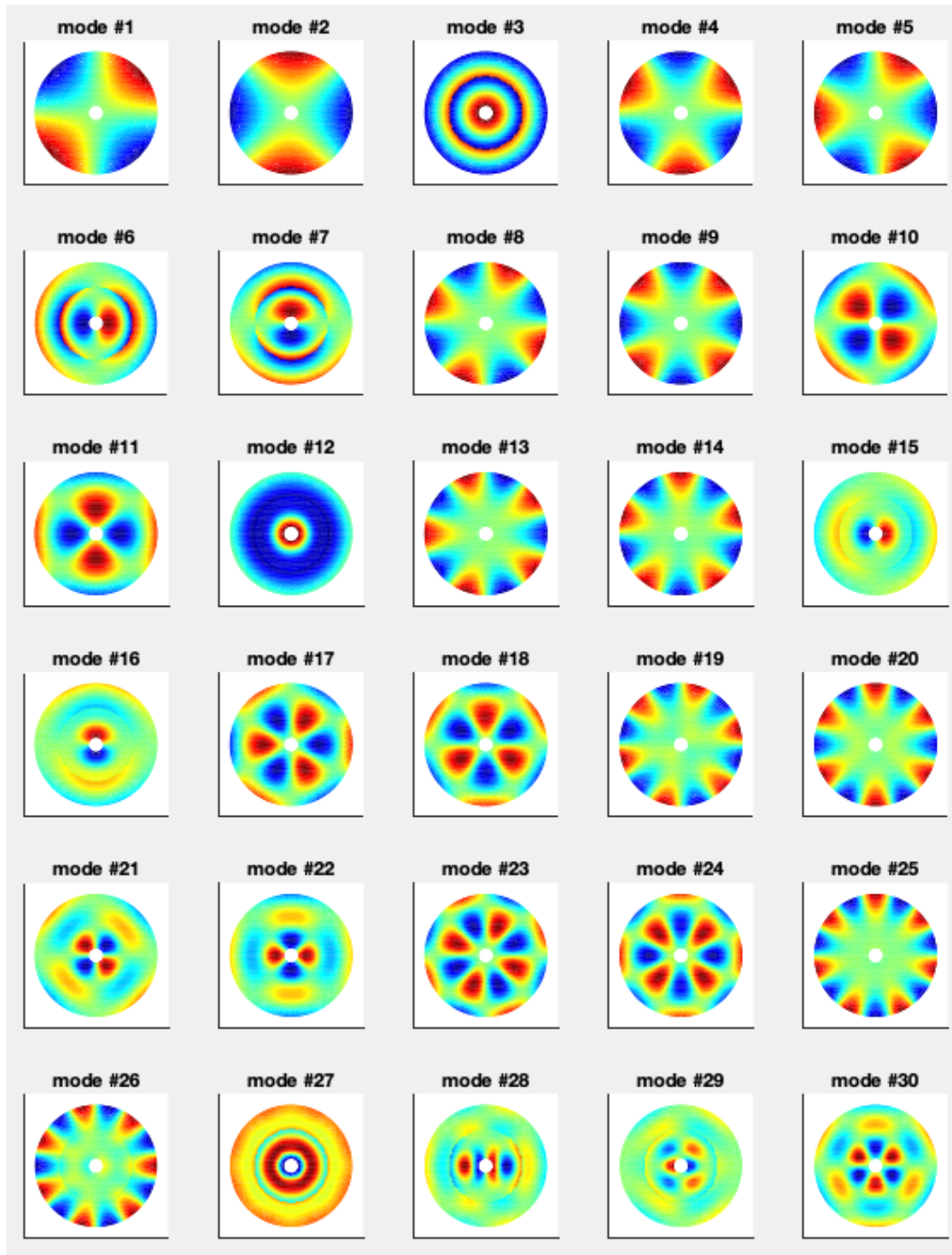


Figure 11: Bending modes determined by the LSST team using the LSST FE model.

We do not want to fill this document with plots. If a reader is interested in looking at other modes, the Python notebooks in the GitHub rep would be a good place to look. All the data files are included in the data package delivered by the Mirror Lab. The path to the files can be found in the Python notebooks.

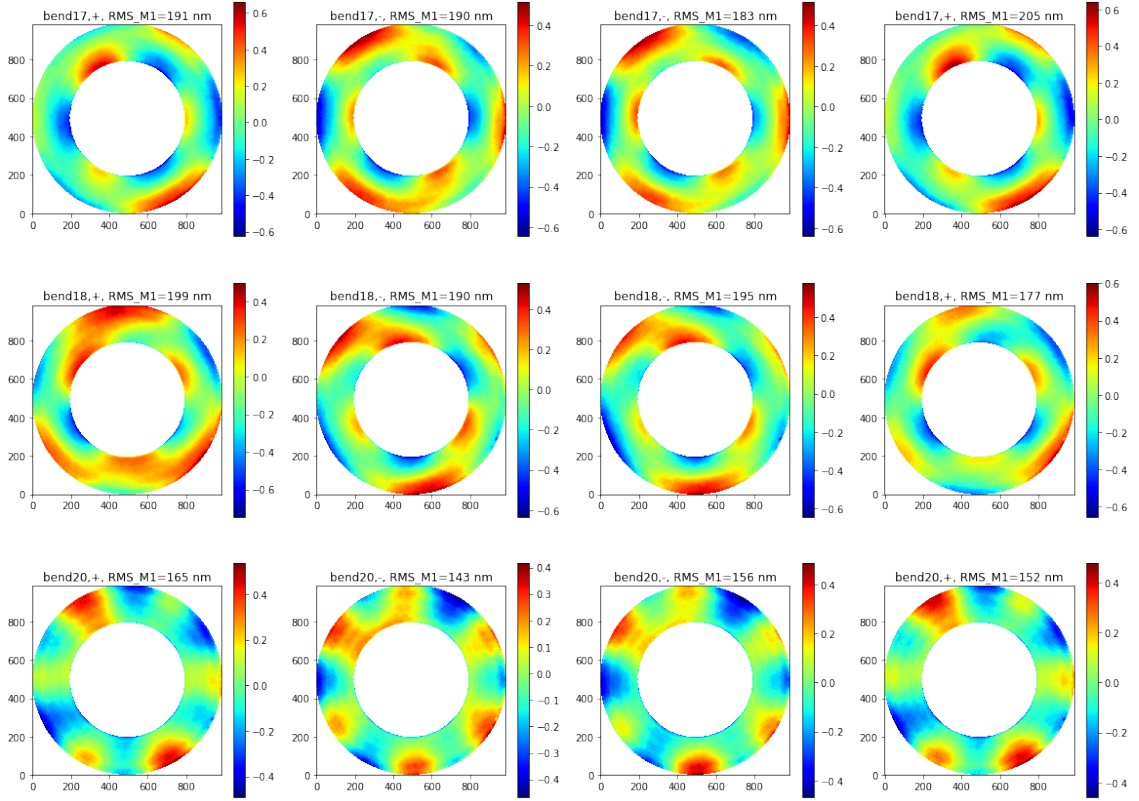


Figure 12: M1 + – – measurements for the LSST bending modes No. 17, 18, and 20.

5.3 Bending Modes Scaling Factors and Cross-Talks

As can be seen from Figure 13 and many other measured bending modes, the measured modes shapes are so much like the FEA bending modes. This gives us confidence that the difference between the measured modes and the FEA modes is mostly a scaling factor, and it is very close to 1.

We next try to determine the scaling factors, and any cross-talk between the bending modes. To do this, we take each measured bending mode B_i , and make a least-square fit using 27 FEA bending modes. The fit gives us 27 coefficients, among which c_i is close to 1, while all the other 26 coefficients should be close to 0. We follow the Mirror Lab analysis, and define the residual of the fit as

$$R = (B_i - c_i B_i^{FEA}) \times \frac{RMS(F_i)}{RMS(F_i^{FEA})} \quad (4)$$

The residual maps for bending modes No. 17, 18, and 20 are given in Figure 14.

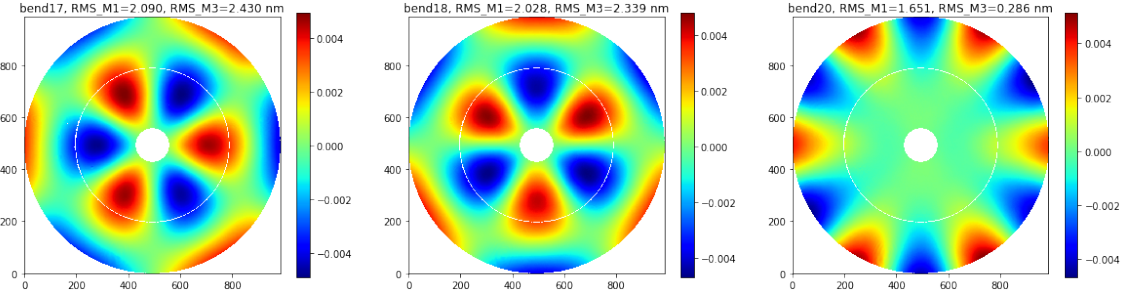


Figure 13: Measured LSST bending modes No. 17, 18, and 20.

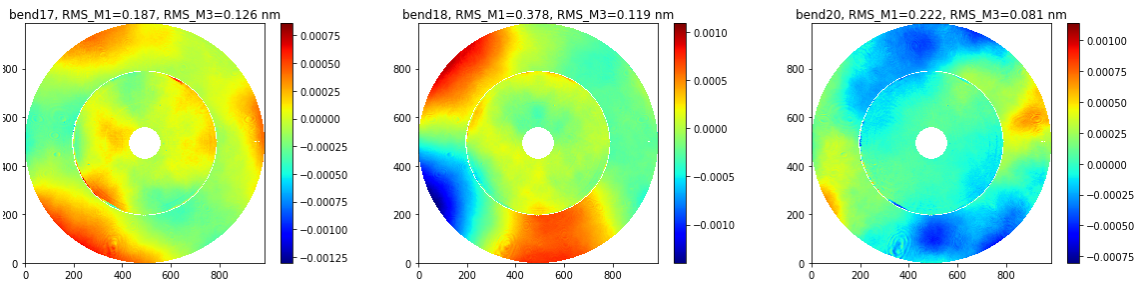


Figure 14: Bending mode residual maps for LSST mode No. 17, 18, and 20.

The c_i 's from the fits, which are the scaling factors that need to be multiplied with the FEA bending modes to make them better match reality, are shown in Figure 15. These scaling factors, for both the LSST bending modes and the Mirror Lab bending modes, are shown together. As another test of the repeatability, four of the the Mirror Lab modes were repeated. The repeated bending modes measurements gave very consistent results on the scaling factors as the original measurements, as can be seen from Figure 15.

A scaling factor less than 1 means FEA model is more flexible than the real mirror. This is true for all the Mirror Lab bending modes. For LSST, the lower order modes (< 15) are generally stiffer than the real mirror. We note that the Mirror Lab analysis report [5] made fits to LSST bending mode measurements using Mirror Lab FEA modes. We believe that that is not meaningful, and could lead to confusion. Due to numerical effect in FE modelling and derivation of the bending modes, the two sets of FEA bending modes look similar but have visible difference, especially in the orientations of the modes. Therefore, the bending mode measurements made using LSST bending mode forces should be fit using LSST bending modes. Otherwise the fits lead to very large cross-talk terms, especially between modes that form pairs, for example, the two astigmatism modes, two coma modes, and so on.

Figure 16 shows the cross-talk matrix of the bending modes, where the j th column, i th row, shows when the force set for the j th bending mode was applied, how much of bending mode i was produced. Most of the low order modes (< 15) are very clean - they are free of contaminations from higher order modes. For higher order modes (≥ 15), the contamination is up to $\sim 15\%$.

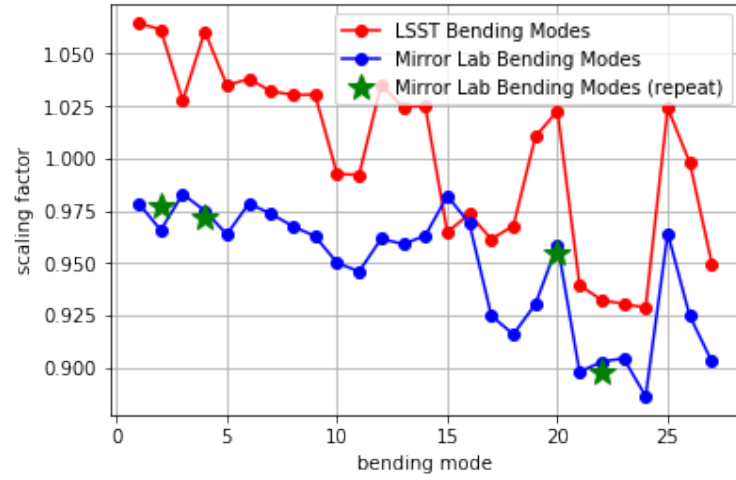


Figure 15: Scaling factors that need to be applied to the FEA bending modes.

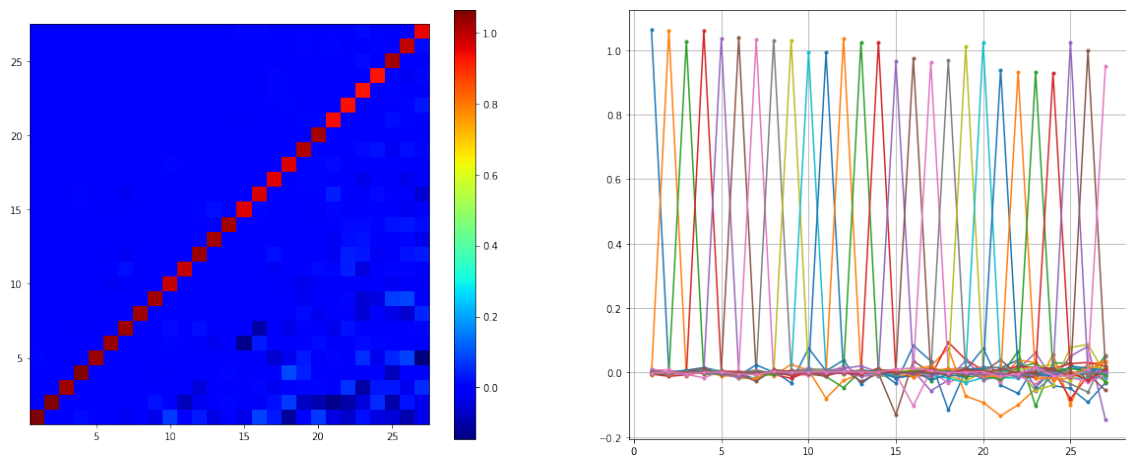


Figure 16: Cross talk matrix between the measured LSST bending modes (left), and the projection onto the column index (right).

Because the FEA bending mode are free of measurement noise, and are much smoother than the measured modes, we choose to apply the scaling factors on the FEA bending modes, and use the scaled modes as the baseline bending modes to go onsky.

5.4 Final Bending Modes

What the cross talk matrix means, is, mathematically,

$$\begin{bmatrix} m1 \\ m2 \\ \vdots \\ m27 \end{bmatrix} = X^T \begin{bmatrix} U1 \\ U2 \\ \vdots \\ U27 \end{bmatrix} = X^T G \begin{bmatrix} V1 \\ V2 \\ \vdots \\ V27 \end{bmatrix}. \quad (5)$$

X^T is the transpose of the cross-talk matrix X . $m1, m2, \dots, m27$ are measured mode shapes. $U1, U2, \dots, U27$ are FEA mode shapes. These are all matrix blocks, each is a nNode x 1 vector. nNode is the number of surface nodes. $V1, V2, \dots, V27$ are FEA force sets. These are matrix blocks too, each being a 156 x 1 vector. G is the FEA influence matrix, which is nNode \times 156.

Noticing that when we applied $V1, V2, \dots, V27$ forces in the Mirror Lab, we measured $m1, m2, \dots, m27$. $X^T G$ actually gives us the real influence matrix (g).

$$g = X^T G \quad (6)$$

We want to keep our mode shapes orthonormal, so we keep using $U1, U2, \dots, U27$ as our bending mode shapes, and scale the forces. Now, what we want to derive is the force sets that would give us $U1, U2, \dots, U27$ in the real world.

$$\begin{bmatrix} f1 \\ f2 \\ \vdots \\ f27 \end{bmatrix} = g^{-1} \begin{bmatrix} U1 \\ U2 \\ \vdots \\ U27 \end{bmatrix} = g^{-1} G \begin{bmatrix} V1 \\ V2 \\ \vdots \\ V27 \end{bmatrix} = (X^T G)^{-1} G \begin{bmatrix} V1 \\ V2 \\ \vdots \\ V27 \end{bmatrix} \quad (7)$$

So, to know $f1, f2, \dots, f27$, all we need to know is the matrix m ,

$$m = (X^T G)^{-1} G = (X^T)^{-1} \quad (8)$$

Note that G is a matrix that applies to the matrix blocks above. Each element of the 27×27 matrix X^T is multiplied with G . Therefore G is commutable with X .

Ideally, we want to make use of the full cross-talk matrix, i.e., multiply the m matrix with the V vectors, to get the final f force vectors which would produce the U bending modes. However, attempting to do so resulted in weird-looking force distributions for the bending modes, as shown in the notebook https://github.com/lsst-sitcom/M1M3_ML/blob/master/finalBendingModes.ipynb.

We therefore decided to set all the off-diagonal elements of m to zero. This is basically saying that we will ignore the measured cross-talks between the bending modes, and assume

those are due to measurement noise and environmental drifts. This is equivalent to using a simple measured scaling factor to scale the forces for each bending mode.

The final bending mode forces after the scaling is found at https://github.com/lsst-sitcom/M1M3_ML/blob/master/data/M1M3_1um_156_force.txt. Each row is for an actuator. There are 156 rows in total. The first column is the actuator ID. The 2nd and 3rd columns are the x and y coordinates of the actuators. The rest of the columns are forces for individual bending modes in Newton. The bending mode shapes are at https://github.com/lsst-sitcom/M1M3_ML/blob/master/data/M1M3_1um_156_grid.txt. Each row is for a surface node. There are 5256 rows in total. The first column is the node ID. The 2nd and 3rd columns are the x and y coordinates in meter for that node. The rest of the columns are for individual bending modes. Note that these are surface normal displacements in meter, which need to be projected to surface sag if used in raytrace programs.

6 Single actuator influence functions

To help better understand the difference between the mirror FE model and the real mirror, we also measured 50 single actuator influence functions. There is nothing special about the number 50. After some number of single actuator influence function measurements, this became a low-priority task. We basically filled the time when other tasks were not ready to be executed. In the end, 50 was what we could get out of the time we had in the Mirror Lab.

The way we determined which influence functions to measure was to pick a set of actuators that represent a variety of types, including number of cylinders, their orientation, and load spreader type, and radial and azimuthal location in the mirror cell. The LSST team made a list of 60 actuator ID numbers, ranked them by priority from high to low, and gave those to the mirror lab crew. The distribution of these 50 actuators are shown in Figure 17 (left), where the same coordinate system as in Figure 1 has been used. We focused on the 4th quadrant, where the actuator ID numbers are in the 100's range. Some actuators in the other quadrants were added to the list, mostly to check symmetry.

The single actuator influence function measurements were done in a very similar way as the bending modes. For each actuator, we take the unit-load forces, as described in Section 5.1, and add a scaling factor so that the FEA-predicted surface would roughly have a RMS of 500 nm. The scaled force for the single actuators, which are also the largest forces among their own unit-load force sets, are listed in Tables 3 and 6 of the Mirror Lab analysis report [5], therefore not repeated here. Just like for the bending modes, we did $+ - - +$ measurements; and we did this for M1 and M3 separately, i.e., M1 surface measurements for a series of scaled unit-load forces, followed by M3 surface measurements for a series of scaled unit-load forces. For the same influence function, the scaling factors were allowed to differ between M1 and M3, to achieve surface RMS of roughly 500 nm in each case.

The fits to the measured single actuator influence functions using their FEA predictions also follow a similar approach as the fits to the bending modes. The major difference is that instead of fitting to 27 bending modes, here the least-square fits are only done using one FEA influence function at a time. Figure 18 shows two examples of such fits, for actuators 102 and 138, representing actuators under M3 and M1, respectively. The first column shows the measured

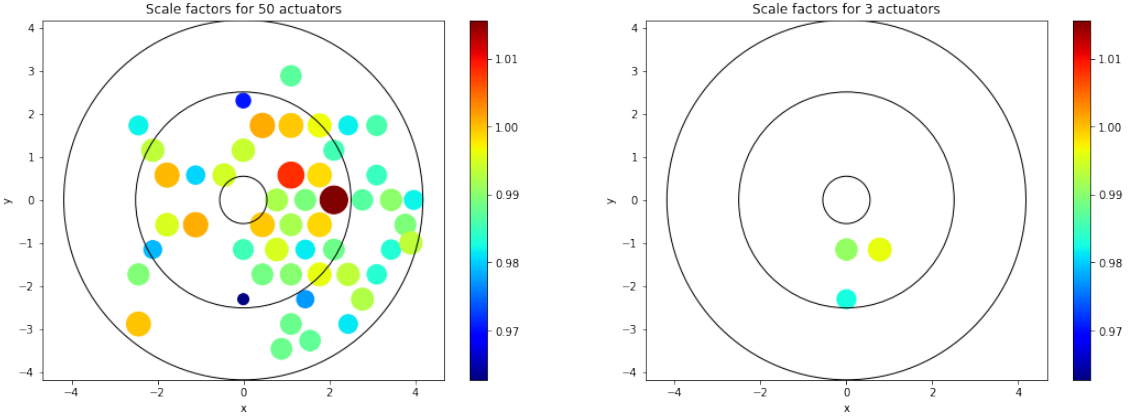


Figure 17: Measured single actuator influence function scaling factors versus their x and y coordinates. These are in the coordinate system as defined in Figure 1. All 50 actuators measured are shown in the left plot, and the right plot shows the 3 actuators that were repeated on a different day. Note that the color scales on the two plots are the same. The size of the circles are relative to other circles on the same plot, therefore not comparable between the two plots.

influence functions. The second column shows the FEA predicted influence functions. The third column shows the fit result, i.e., the fitted scale factor times the second column. The fourth column shows the residual of the fits, scaled to 1N of RMS force on the selected actuator. The circles indicate the locations of the selected actuator. Good agreement between the measured influence functions and the FE model was seen, in terms of both the magnitude and overall shape. The scale factor for actuator 102 was determined to be 0.989, and for actuator 138 it was 0.988.

It was observed that for all actuators under M3, the residual maps have localized spots that are negative (blue). This implies that the real mirror is stiffer against shear than the FE model. For M1, the residual maps generally show more blue than red on or around the selected actuator positions. But the locality is much less pronounced.

Note that the single actuator measurements were done only using the Mirror Lab FEA influence functions. Since we do not use the results presented in this section in any quantitative calibration of the FE model or the final bending modes, we did not make comparisons between the Mirror Lab FEA influence functions and those derived from the LSST FE model, nor the force vectors for those single actuator influence functions between LSST and the Mirror Lab. We did not repeat the influence function measurements (if the unit-load forces are different) for LSST influence functions.

The values of the scale factors to be applied to the FEA single actuator influence functions are shown in Figure 17 (left). The scale factors to be applied to the FE influence functions range between 0.96 – 1.02. To check the repeatability of these measurements, we redid these for three actuators on a different day. The results on are shown in Figure 17 (right).

All results in this section show consistent agreement between the FEA single actuator influence functions and those measured for the real mirror. The detailed analysis in Jupyter

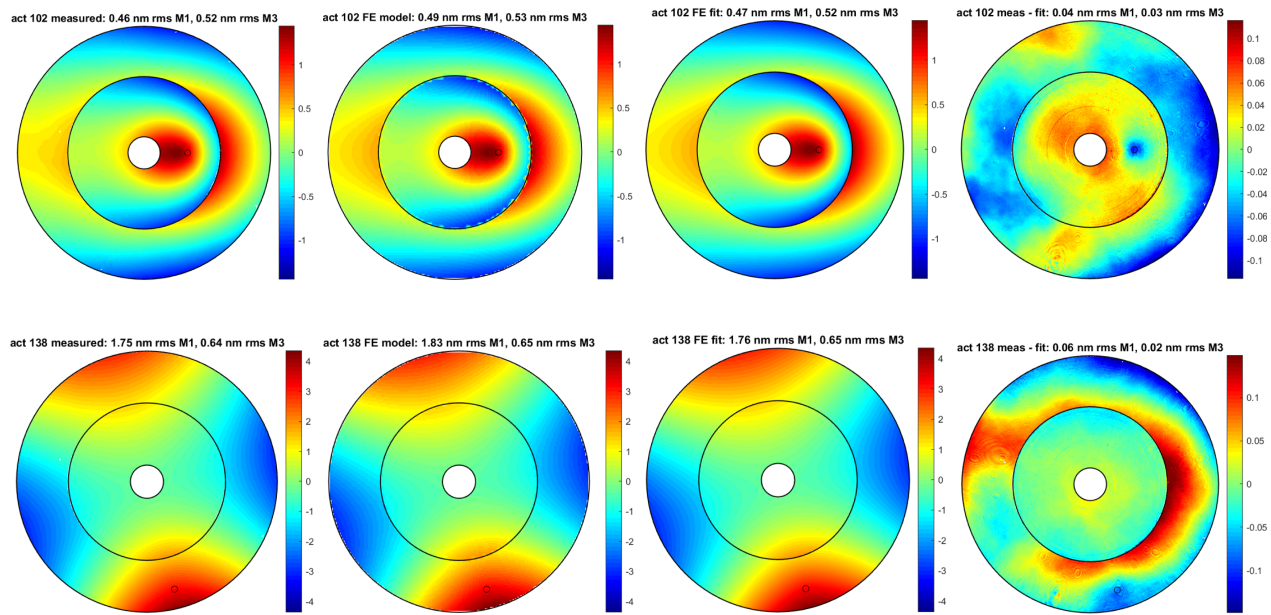


Figure 18: Measured single actuator influence functions (1st column), the corresponding FEA predicted influence functions (2nd column), the fitted surfaces to the FEA influence functions (3rd column), and the residual of the fit (4th column) for two example actuators - 102 (top row) and 138 (bottom row).

Notebook format is documented in

- https://github.com/lsst-sitcom/M1M3_ML/blob/master/190118.ipynb
- https://github.com/lsst-sitcom/M1M3_ML/blob/master/190122.ipynb
- https://github.com/lsst-sitcom/M1M3_ML/blob/master/190214.ipynb
- https://github.com/lsst-sitcom/M1M3_ML/blob/master/190218.ipynb

7 Surface optimization

The surface optimization was what took the most time in the Mirror Lab. But at the end, we achieved superb surfaces on both M1 and M3. We will present the results later in this Section 7.3. Looking back at the whole process, from turning on the system at the beginning of the test campaigns to eventually achieving the final optimized surfaces, here is a list of key things that we had to do to get there.

1. M1M3 global optimization
2. use of LSST bending modes
3. correct calculation of the initial forces
4. understanding the divits above the quads
5. understanding the absolute offset in actuator forces
6. use of bending modes up to 27

No 1 and 2 above are the easiest to explain. We describe them here in a bit more detail, then go through 3 - 6 in the sub-sections. The analysis is spread into many notebooks. We will refer to those where relevant.

Initially we only iterated the optimization process using M1 surface measurements, but only to find that M3 drifted a lot during that process. So we decided to do the M1-M3-M1 measurements, then fit the M1M3 combined surface to the M1M3 combined bending mode shapes. Note that when the mirror was polished back in circa 2014, the Mirror Lab was able to polish M1 first, fit M1 surface to low order bending modes, then use those bending modes as the target shape during M3 polishing. That was because the data processing at that time included thermal corrections. So the mirror shape measured then were always in reference to the shape in a pre-defined thermal condition.

At the beginning of the surface optimization process, we used the Mirror Lab bending modes. At some point we decided to give the LSST bending modes a try. The LSST bending modes appeared to be more effective while used in these optimizations. They resulted in somewhat better surfaces, and the convergence toward better surfaces were noticeably faster. We do not think the LSST bending modes are inherently superior in any way. As we mentioned earlier,

we believe the bending mode derivations are identical between LSST and the Mirror Lab. So the difference in these two sets of bending modes most likely reside in the two different FE models that were used. It may be that the LSST FE model went through many refinements and have better representation of the material properties.

7.1 Initial force calculation

The plan was to start the surface optimization with the support forces from the 2014 acceptance testing. Then, hopefully the surface shape change due to the different thermal environment can be taken care of using 20 or so low order bending modes. However, we shouldn't just use the support forces the way they were in 2014, because some of the mirror support hardware have changed between then and now. The initial force calculation has to take that into account.

This calculation may sound trivial - starting from the 2014 forces, one simply removes the weights of the Mirror Lab hardware which had been removed since then, and add the new LSST hardware weights. Based on that, we put together a Notebook - https://github.com/lsst-sitcom/M1M3_ML/blob/master/sec3.2InitialForces.ipynb. However, this is not as simple as one might first think, mostly because the Mirror Lab actuators were all SAAs, while most of the LSST actuators are DAAs. With the secondary cylinders of the DAAs oriented at 45° relative to the primary, we have to command some non-zero forces on the secondary cylinder, to keep the primary cylinder at vertical position, just like when the DAAs are free-standing. The actual mathematical derivation of the initial force set is rather tedious, therefore not documented here. Instead, they are found in a separate document, Document-32192 [8]. That document also gives analytical results for off-zenith pointings. These will need to become part of the M1M3 look-up-table (LUT). The numerical calculations are found here - https://github.com/lsst-sitcom/M1M3_ML/blob/master/sec4.3InitialForces.ipynb.

7.2 Divits above the quads

Very early on in the test campaigns, even where we used M1 only for the surface optimization, we observed 4 low spots on the M3 surface, roughly right on top of the four actuators whose load spreader has 4 pucks. We call those four actuators the quads. Figure 19 shows the optimized M1 and M3 surface together from an optimization on 2/12. This particular optimization was done using the Mirror Lab bending modes, and was an M1M3 global optimization. Four dark blue spots can be clearly seen on top of the quads. See https://github.com/lsst-sitcom/M1M3_ML/blob/190212.ipynb for more details.

Our first reaction was that there is some kind of force offset that was not properly accounted for. And, irregardless of the reason, just bumping up the forces on the quads should fix it. It turned out that simply increasing the forces on the four quads didn't work out very well. Just looking at the depth of these low spots, and using the single actuator influence functions, we could estimate how much forces would be needed to bring these spots up. Figure 20 shows the M1M3 surface we got by adding 350N to the outer quads, and 300N to the inner quads, then optimizing using 27 Mirror Lab bending modes. The divits seem to be less visible, but the

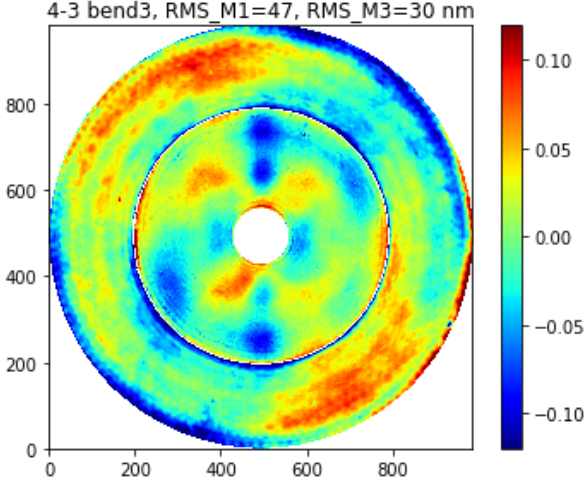


Figure 19: Measured M1M3 surface on 2/12, where no additional forces were added to the quads, and optimization was done using 27 Mirror Lab bending modes.

overall RMS on M1 and on M3 did not get better, as shown in the titles of these plots. This is also found in https://github.com/lsst-sitcom/M1M3_ML/blob/master/190212.ipynb.

Another problem we ran into with simply increasing the forces on these quads was that we kept triggering the safety limits of the M1M3 control software, specifically, the near neighbor check. In order to avoid the situation where one actuator is acting dramatically differently from its N near neighbors, which could impose a danger to glass safety, we require the force on any single actuator to be within a certain range from the average of its N neighbors. Most of the time we have $N = 6$.

$$F_i - \frac{\sum_{j=1}^N F_j}{N} <= c \frac{W_{M1M3}}{156}. \quad (9)$$

W_{M1M3} is the weight of the mirror. We have $W_{M1M3} \approx 167,000$ N. By default, we set $c=1$. So this requires the above difference to be less than ~ 1070 N. If the above condition is triggered then the mirror goes into a fault state - the mirror will be lowered, and we have to start over by raising the mirror. In addition to the near neighbor check, there are also other safety checks, including the moment check, weight check, Active Optics force check, and a far neighbor check. The far neighbor check is very similar to near neighbor check, with $N = 12$. It is aimed at protecting the mirror from large global bending.

Of course, we thought hard on what could be causing these so localized features. In other words, what could have changed between mirror acceptance in 2014 and 2019, that lead to such difference in the mirror surface shape. With the analysis described in Section 7.1 and Ref [8], for a while, we believed we had accounted for everything properly. Then we started questioning the absolute force calibration of these actuators. The relative force calibration was done before the individual actuators were installed, meaning that we are pretty confident when we command an actuator to increase the force by dF , the load cells show the increase is $dF + e$, where e is fairly small in this context, according to Section 9, the actual force increase is not far from dF either. But, could the absolute calibration be so much off, i.e., when we think we

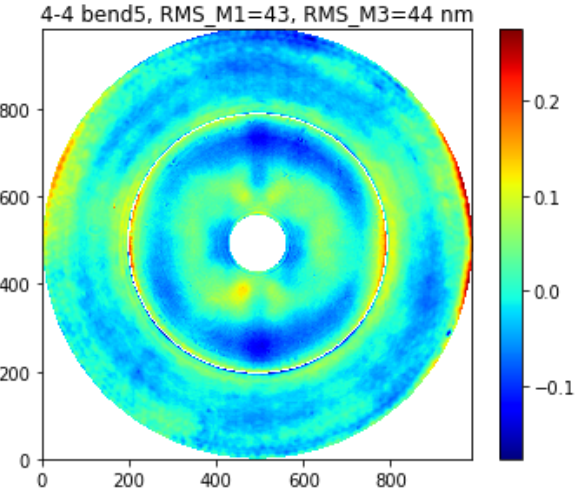


Figure 20: Measured M1M3 surface on 2/12, where we added 350N to the outer quads, and 300N to the inner quads, and optimization was done using 27 Mirror Lab bending modes.

are applying 1800 N force, it is actual only outputing 1500 N? That sounds impossible, because all these DAAs are the same. We cannot think of a reason that the DAAs installed under the quads are so much off while other DAAs installed under the triples have offsets that are close to zero. Still, since we had a few spare DAAs laying in the lab, we conducted some measurements by letting these free-standing DAAs, without any loads, to stand vertically, and also lay on their sides. Then we measure the load cell readings. The results are documented in Ref. [9] where they are also compared to analytical calculations found in Ref. [8]. Good agreement was found. This resulted in a future to-do item, which is to measure the absolute force offset of all the load cells after all the actuators are detached from the mirror back surface. The actuators will need to be detached for shipping to Chile anyway.

We also noticed that these localized features on the mirror surface, are actually of higher spatial frequency than the actuators could possibly correct. Figure 21 shows the surface we get if we take the surface measured, as shown in Figure 19, fit to all 153 bending modes, then subtract off the result of the fit. Note that we have 153 bending modes because the bending modes have to satisfy 3 constraints: z net force is zero, and x and y moments are zero. This is basically saying, Figure 21 shows the best surface we could possibly get by adjusting all the actuators. The surface RMS values are small, but the pattern on the surface is still visible. So this is higher spatial frequency than the actuators can create or compensate. More details are found in https://github.com/lsst-sitcom/M1M3_ML/blob/master/190212.ipynb.

Eventually, we figured out that it must be due to the following: there has been a change in the way the quads are supported. Due to mirror design, these quads require larger forces than other actuators to support the mirror against gravity. That is why they are quads - with 4 pucks. During mirror polishing, the Mirror Lab did not have strong enough actuators to be used under these quads, so they used two actuators under each quad. That is why, as mentioned in document-32192 [8], the Mirror Lab initial force set had 160 values, and they had 160 interface plates. The two actuators for each quad was on the two sides of the load spreader. With the

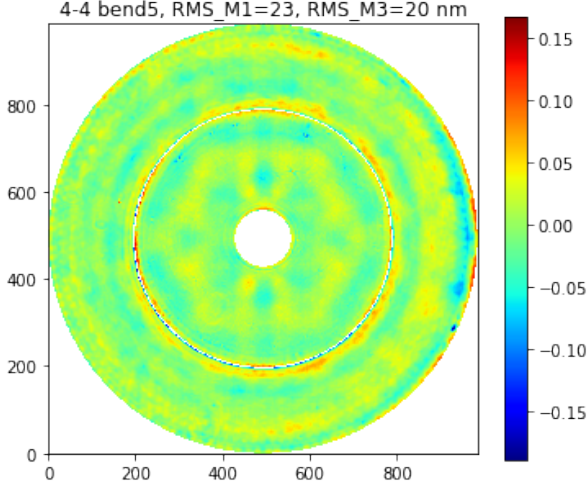


Figure 21: FEA prediction of best M1M3 surface we could achieve by force optimization. This was obtained by taking the measured surface as shown in Figure 19, make fit to, then remove all 153 bending modes.

LSST mirror cell, those pairs of actuators were replaced with single DAAs, which supports the 4-puck load spreaders at the center. In the later case, the load spreaders acted like bridges. With support forces around or larger than 1500 N, lateral forces and moments are created, which push the contact points on the mirror back surface outwards. As a result, low spots are created on the front surface.

Optimizing the mirror surfaces with the FE model gave roughly same forces as those as used to produce the surfaces shown in Figure 19. To be specific, we subtracted the forces used to produce the surfaces shown in Figure 19 from the FEA predicted optimized forces. When we looked at the force difference map, we didn't observe any large spikes around the quads. This is because the shear forces and moments are not present in the finite element model. The finite element model does model the pucks of the load spreaders. But all it does is to evenly distribute the forces applied by individual actuators onto the pucks, by treating the load spreaders as perfectly rigid.

To check whether the lateral forces are the real cause here, Ed Hileman modeled the individual load spreaders as flexible structures. Shear forces were derived from the FE model, with typical large axial forces exerted on the load spreaders. These shear forces are then added to the mirror FE model together with all the other actuator forces. The resulting M1 and M3 surfaces were shown to be very close to the actual measured surface with the 4 divits. For readers' convenience, the modeled surfaces with lateral forces are also included here, in Figure 22.

Ideally, we would want to go back and change the load spreader design, to avoid these unintended shear forces and moments. However, given that the actuated tests have already been performed using these hardware, and we've already achieved pretty good optimized M1 and M3 surfaces, going back to change the design would invalidate all the test results. Changing the hardware design would also invalidate the single actuator influence function measurements for the quads, and also bending modes, to some extent. We therefore choose to use the load

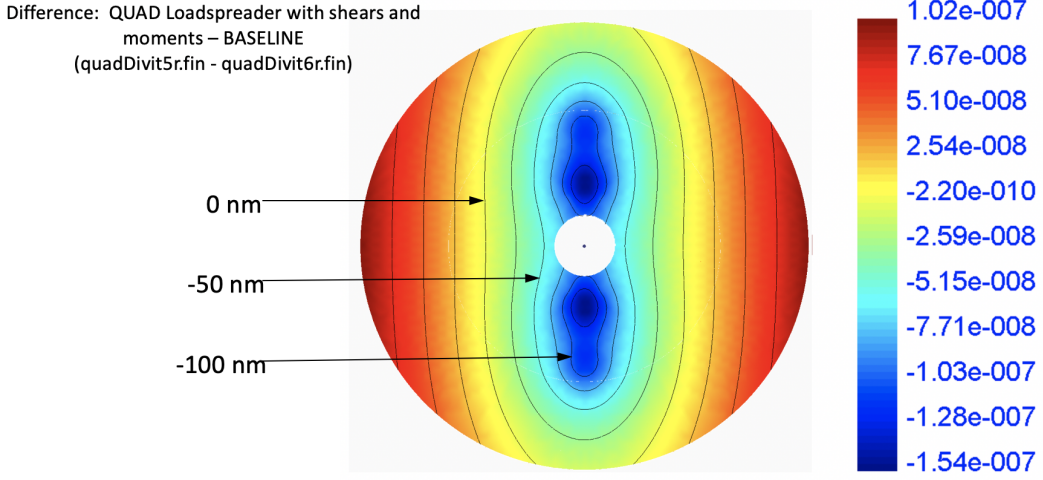


Figure 22: FEA prediction of M1M3 surface shape due to shear forces and moments associated with the four quads.

spreaders and the actuators the way they are.

7.3 Final Optimized Surfaces and Forces

After understanding the root cause for the divits on top of the quads, it became obvious why we could not further improve the surfaces by adjusting actuator forces.

As the final push for better surfaces, we ran another round of optimization on the last day of test campaign No. 2, by making a fit to the measured M1M3 surfaces using 14 single actuator influence functions. These 14 influence functions included the quads, their neighbor actuators on both sides in the $\pm x$ direction, plus actuator No. 101 and 301. As expected, some small further improvements were achieved by adjusting these 14 actuator forces. After two iterations, the fit to the 14 influence functions yielded forces that were close to zero.

Looking back at the entire surface optimization process, a few times we got to, or got close to, the best optimized M1 and M3 surfaces.

- On 1/25, the last day of test campaign No. 1, using incorrectly calculated initial forces, Mirror Lab bending modes, and additional forces on the quads, we got to 33 and 28 nm RMS on M1 and M3, respectively. For historical reasons, we refer this force set as f_1 .
- On 2/14, the 4th day of test campaign No. 2, where we had started using the correct initial forces, and using LSST bending modes, with no additional forces on the quads, we reached 30 and 26 nm RMS on M1 and M3, respectively. we refer this force set as f_3 .
- On 2/21, the last day of test campaign No. 2, for the final round of surface optimization, we started from f_3 . We call it iteration 0. For iteration 1, the surface RMS values were 28/24 nm. We refer to this force set as f_a . The force change between iteration 1 and 0 was up to ~ 150 N, on the quads.

- On 2/21, for iteration 2, the surface RMS values were 31/20 nm. We refer to this force set as fb . The force change between iteration 2 and 1 was up to ~ 100 N, on the quads.
- On 2/21, for iteration 3, the surface RMS values were 27/21 nm. We refer to this force set as fc . The force change between iteration 3 and 2 was up to ~ 0.2 N, on the quads.
- On 2/21, by the end of the day, we measured the surfaces again by applying fc . Thermal conditions had drifted a bit by then. We reoptimized the M1 and M3 surfaces using 27 LSST bending modes. With 3 iterations, we got surface RMS values of 28/20 nm. We refer to this force set as fd .

The M1 and M3 surfaces, as produced by the above force sets, are shown in Figure 23. The differences between them are small. These are also documented in

- https://github.com/lsst-sitcom/M1M3_ML/blob/master/190125.ipynb
- https://github.com/lsst-sitcom/M1M3_ML/blob/master/190214.ipynb
- https://github.com/lsst-sitcom/M1M3_ML/blob/master/190221.ipynb

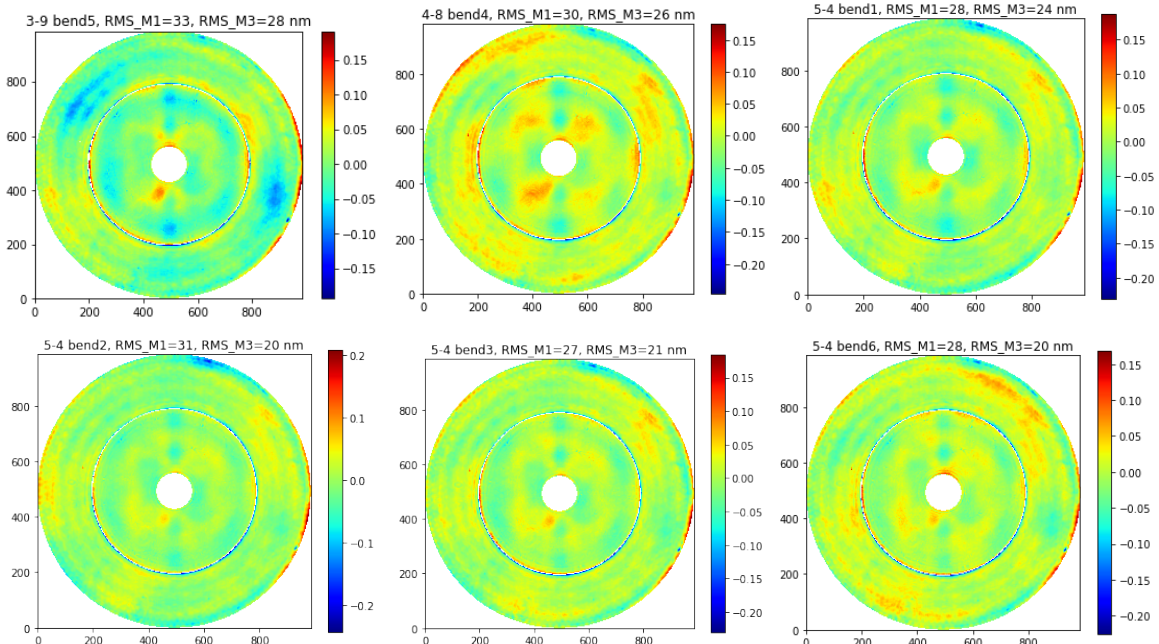


Figure 23: The M1 and M3 surfaces, as produced by force sets $f1$, $f3$, fa , (top row, from left to right), and fb , fc , fd (bottom row, from left to right).

7.4 M1M3 Structure function

See Figure 24 for the M1 and M3 structure functions (SF) calculated for the surfaces produced with the fc force set above (27nm on M1 and 21nm on M3). We also compare to three other curves as references:

- The (2014) polishing specifications.
- The SF for the 2014 polished surfaces.
- Revised (2019) specifications, by adding image quality allocations for temperature and force accuracy to the polishing specification. (note that we are using all the thermal allocation here: 54 mas for M1 and 54 mas for M3; and the 10 mas for force accuracy have been divided equally between M1 and M3. We left out the 10 mas budget for M1M3 vibration, since no cooling fans were installed).

For both mirrors we are meeting the SF specifications. For M1, the SF increased pretty uniformly across the spectrum. This is true for both the specification curves and the measured SF. For M3, the increase in the measured SF is much more significant in the range roughly between 0.05m and 0.5m. At one point ($\sim 0.1\text{m}$ separation) it is basically touching the specification curve.

7.5 Image Quality Evaluation

We took the M1M3 surfaces produced with the fc force set above (27nm on M1 and 21nm on M3), and inserted into the LSST optical design Zemax model (v3.3), to directly evaluate the impact of such a surface on the system image quality. The detailed procedure follows exactly what is described in document-17171 [1]. Wavefronts, in the form of 2048×2048 OPD maps, are evaluated at 31 Gaussian Quadrature (GQ) field points. These are then used to evaluate the Normalized Point Source Sensitivity (PSSN), changes in the 5σ imaging depth (Δm_5), effective full-width at half maximum (FWHM), and FWHM.

The results for ideal optics with the fc surfaces are shown in row q of Table 1. Rows a and g are copied from Document-17171 [1]. We use Δ for the differences between the fc surfaces and the 2014 polished M1M3 surfaces. Polishing in 2014 was done on static supports. Therefore, Δ has contributions from both the mirror support system and thermal factors. When we do the subtraction between two rows, we take the ratio of the PSSN values, then convert the resulting PSSN into Δm_5 and effective FWHM ($FWHM_{\text{eff}}$). The subtraction of FWHM is done by subtracting in quadrature.

The numbers in the parentheses are image quality budgets in FWHM. For Δ , these are actually the upper bonds. The 77mas is the quadrature sum of 54mas (for M1 thermal), 54mas (for M3 thermal), and the 10mas (for M1M3 actuator force accuracy). Because further thermal FEA analyses were done after these budgets were put in place, the current best knowledge is 69mas for M1 thermal and 84mas for M3 thermal. If we use these values then we get 109mas for the quadrature sum. We left out the 10 mas budget for M1M3 vibration, since no cooling fans were installed.

7.6 Use of bending mode No. 27

The test plan before the test campaigns started was to measure 22 bending modes. The surface optimization was also planned to be performed using 22 bending modes. However, during the

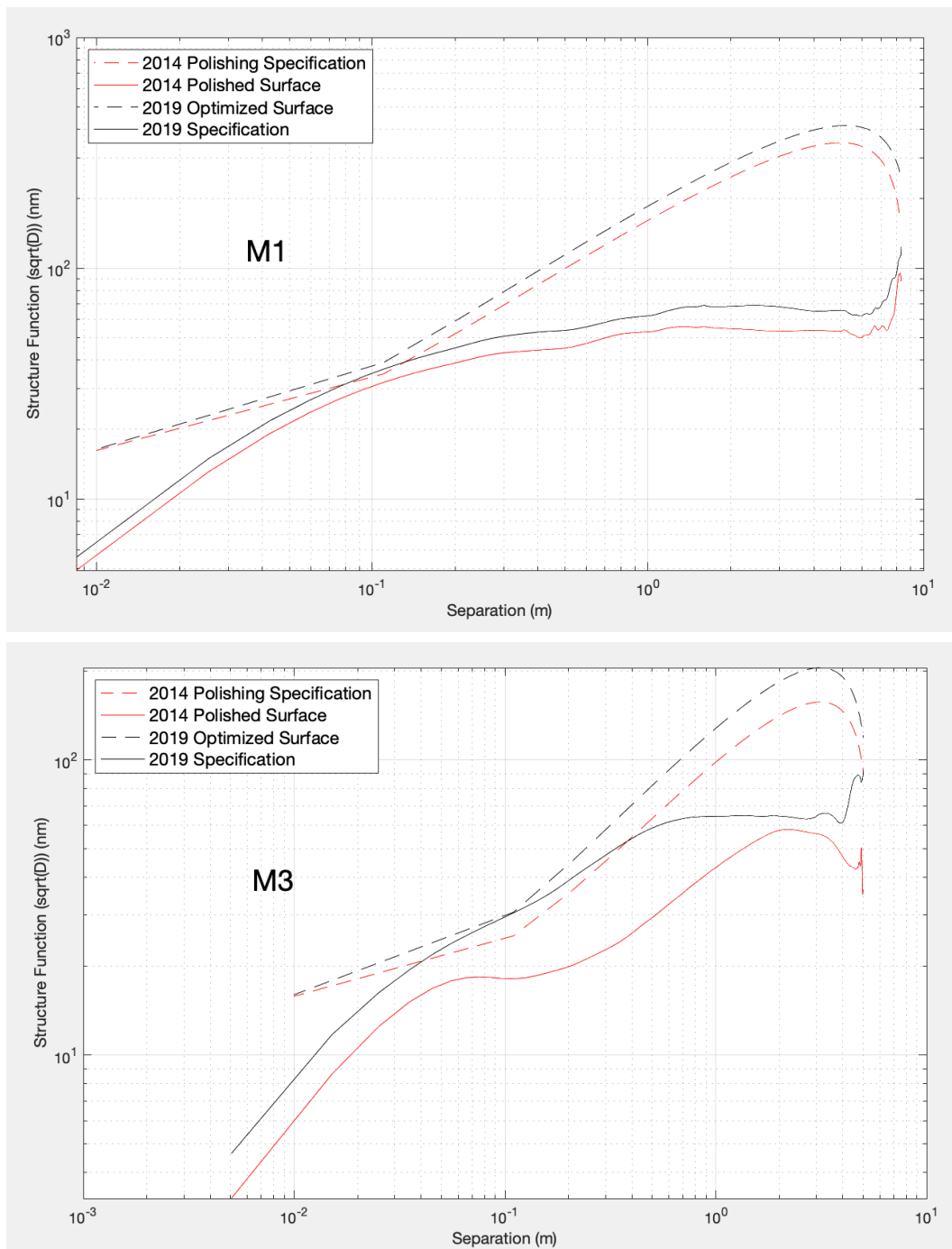


Figure 24: The M1 and M3 structure functions, and comparisons to the 2014 polished surfaces, and their corresponding specifications.

Table 1: Summary of PSSN, Δm_5 , $FWHM_{\text{eff}}$ and $FWHM$ for various optical configurations of the M1M3. All numbers shown are GQ values across the 31 field points as defined in Ref. [1]. The numbers in the parentheses are image quality budgets in FWHM.

		PSSN	Δm_5 (mmag)	$FWHM_{\text{eff}}$ (mas)	$FWHM$ (mas)
a	Ideal Optics	0.9787	12.0	96.1	100
g	=M1M3 Polishing (no crows' feet)	0.9317	38.5	178.4	112 (112)
q	=a+g+ Δ	0.9083	52.2	224.1	164
r	=g+ Δ = q-a	0.9137	49.1	200.3	129
Δ	= r-g	0.9807	10.6	91.5	64 (77 109)

surface optimization, it was observed at, when we started with the calculated initial forces, we were often left with a residual that looked like bending mode No. 27. At that point we decided to include bending mode 27 in the surface optimizations. And we measured bending modes up to No. 27, for both the Mirror Lab bending modes and the LSST bending modes.

Now the question is, do we need bending mode 27 for AOS closed-loop? Ref. [10] attempts to address this question, by looking through the entire surface optimization - under what circumstances did we need to include significant amount of bending mode 27 to improve the surfaces. The conclusion from Ref. [10] is that bending mode 27 was only needed right after we started a round of surface optimization with calculated initial forces. If the starting force set already included bending mode 27, it won't be needed for subsequent optimizations. What that says is basically that we need bending mode 27 to go from the initial calculated force set to the optimized force set. On top of the optimized force set, additional environmental drift will not require a correction with bending mode 27. In other words, bending mode 27 is part of the static correction. It is not dynamic, and will most likely not be needed during day-to-day AOS operations.

However, considering we have only been able to optimize the M1M3 surfaces at zenith, and when we go off-zenith, we would be mostly relying on the FE model, we will include bending mode 27 in the AOS bending modes. Since the AOS software has been set up to use 20 M1M3 bending modes, we will keep the total number to be 20. The actual set of bending modes used will be 1-19, and 27. Note that bending modes 19 and 20 are a symmetric pair, with 6θ azimuthal dependence. We do not measure 6θ Zernikes terms (Z_{27} and Z_{28}) with our wavefront sensors anyway. Bending mode 19 will likely not be used either, which we can easily truncate off with the truncation of the optical sensitivity matrix.

7.7 Building the LUT

In coming up with the LUT for zenith pointing, we want to average the above force set, or a subset of them, so that we can average out measurement noise to some extent. Since $f1$ had additional forces on the quads, while others do not, it is not good to be included in the average. $f3$ was before we started optimizing using 14 influence functions, so it is a bit different from the rest of the force sets. So we leave that out as well. fa should not be included either

because it is in the middle of optimization with 14 influence functions, before things completely converged. fb and fc were after the convergence. There were literally no difference between fb and fc . The difference between fd and $(fb + fc)/2$ was a combination of the first 27 bending modes, actually dominated by the two astigma modes. These were due to temperature drifts. Considering that when we do this on the summit the temperate profile will be different anyway, we take the average of fb , fc , and fd , and use it as the final zenith-pointing LUT. The analysis is documented in https://github.com/lsst-sitcom/M1M3_ML/blob/master/finalLUT.ipynb.

To extend the LUT to off zenith, we need to combine the optimal forces at zenith and those at horizon. The optimal forces at an arbitrary zenith angle θ_z has three components,

$$F = F_G(\theta_z) + F_B + F_a(\theta_z), \quad (10)$$

where F and each term on the right are 156×1 vectors. The first component F_G is the force that is needed to counter gravity of the glass mirror itself. It has a simple dependence on θ_z .

$$F_G(\theta_z) = F_{Gz} \cos \theta_z + F_{Gh} \sin \theta_z. \quad (11)$$

The 2nd component is a static bending force. The 3rd component is due to actuator weights, hence has a special θ_z dependence, as shown in Eq. (19) and (20) of Ref. [8].

By doing this optical testing of M1M3 in the Mirror Lab, we know F_{Gz} , F_B , and F_a . But since we did this at zenith only, where $\sin \theta_z = 0$, we couldn't learn anything about F_{Gh} , hence the case for further horizon testing of M1M3 on the summit. For horizon testing, we know $F_a(\theta_z = 90^\circ)$ and F_B , we will be able to fine-tune F_{Gz} , by starting with the FEA-predicted horizon forces. Note that the FEA-predicted horizon forces will correspond to F_{Gh} , instead of F in Equation (10), because the FEA models a perfectly polished mirror, so there is no F_B needed, and the FEA doesn't know anything about F_a .

The notebook https://github.com/lsst-sitcom/M1M3_ML/blob/master/get_Fxyz_from_EFD_190125.ipynb illustrates the different components of the forces at zenith, as defined by the M1M3 control software, in the order they were added during the testing,

- A 2014 polishing forces – removed Mirror Lab hardware + installed LSST hardware;
- B forces due to lateral actuator weights;
- C static bending modes needed in 2014 to theoretically bend the mirror into optimal shape;
- D Force Balance (FB) forces for cancelling out any nonzero net forces and moments;
- E Bending mode forces applied during optimization;
- F Additional single actuator influence function forces applied during optimization.

Among these components, A is for countering gravity. D is in principle due to gravity as well. But it is closely related to the mirror as positioned relative to the mirror cell. What we measured in the Mirror Lab applied to the mirror positioning in the Mirror Lab. Considering that the actuators are being reinstalled in Chile, and these forces are small, and they will be reapplied

automatically by the force balance system, we leave them out in the LUT. F is indirectly due to gravity - gravity requires large support forces on the quads which leads to deformation of the load spreaders. We expect F not to go to zero at horizon pointing, because there will still be nonzero F_z to stop the mirror from tipping over. But those forces will be much smaller. And the nonzero effect will be taken into account by F_{Gh} when we do the optical testing at horizon.

$$F_G(\theta_z = 0) = A + F. \quad (12)$$

Obviously,

$$F_a(\theta_z = 0) = B. \quad (13)$$

C and E are about bending the mirror into optimal shape. Together they make up

$$F_B = C + E. \quad (14)$$

On the other hand, the M1M3 control software publishes the force values and their components as part of the telemetry, at a frequency of 50 Hz. These are captured by the EFD. The relevant data tables are

- K1 = D = *m1m3_logevent_AppliedBalanceForces*
- K2 = C = *m1m3_logevent_AppliedStaticForces*
- K3 = E = *m1m3_logevent_AppliedActiveOpticForces*
- K = A+B+C+D+E+F = *m1m3_logevent_AppliedForces* or *m1m3_logevent_AppliedCylinderForces*

Therefore,

$$F_G(\theta_z = 0) = A + F = K - B - C - D - E \quad (15)$$

The notebook https://github.com/lsst-sitcom/M1M3_ML/blob/master/finallUT.ipynb shows the numerical derivation of the LUT. The results are duplicated in Figure 25. Once we've done the M3 horizon testing on the summit, we will simply replace the FEA-predicted F_{Gh} with measured to get the updated LUT.

Document-34826 [11] gives the AOS force budget. For M1M3, this can be summarized as

- The z-force has 4 components: Wavefront closed-loop (445N), slewing (150N), dynamics (5% of total), and LUT (the rest);
- The y-force has 3 components: slewing (400N), dynamics (5% of total), and LUT (the rest);
- The x-force has 2 components: slewing (600N), dynamics (5% of total). Yes, the remaining budget is unaccounted for.

We note that the forces calculated in this section all go into the “rest” category. For the x-forces, Figure 25 (left) shows we need nonzero, but small x forces in the LUT. The assumption is that these allocations are just guidelines, which will not be strictly enforced by the control software. Therefore, the x-force budget above does not have a LUT component.

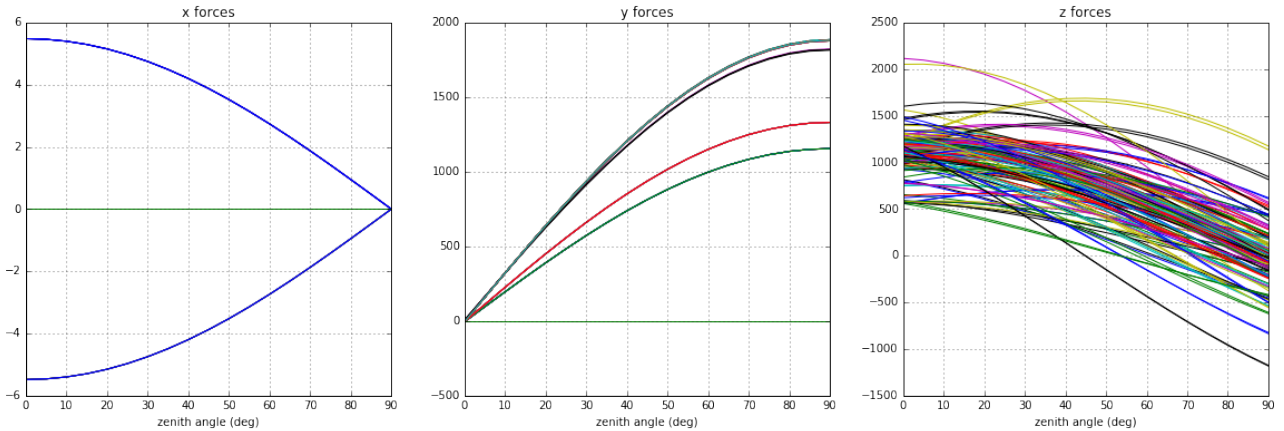


Figure 25: The M1M3 LUT based on Mirror Lab test data at zenith pointing and FEA analysis at horizon pointing.

8 Horizon tests

Even though the testing at the Mirror Lab was only for zenith pointing, we hoped to gain some knowledge about the mirror at horizon pointing. As we discussed in Section 7.7, it is understood that F_{Gz} and F_{Gh} are independent components, so we can not simply learn about one and determine the other, however, there are two things we could do at zenith pointing to help us get better informed with the upcoming horizon testing on the summit. These are described in the following two subsections.

8.1 Horizon Bending Test

At horizon pointing, if we do not apply any axial force, i.e., let all $F_z=0$, then the mirror is going to sag. The effect of applying the horizon optimized forces, F_{Gh} , is to correct that sag. Without gravity pulling perpendicular to the optical axis, the F_{Gh} would produce a surface shape that is the inverse of the horizon gravitational sag. So, we could apply the FEA-determined F_{Gh} in the Mirror Lab, measure the resulting surface shape, then compare to FEA prediction.

Since the gravity is still going downward, this is essentially still a bending test, i.e., these horizon forces we apply are nothing but a particular combination of bending mode forces. We are not really testing the behavior of the mirror at horizon pointing. Instead, we are testing we can apply that particular force pattern, and see if it produces a shape that resembles the FEA prediction.

There is still one subtlety here though. The horizon forces F_{Gh} has a net x -moment. The reason is that the DAA pivot points are on a different $x - y$ plane from the center of gravity of the mirror. The axial forces have to produce a net x -moment, to prevent the mirror from tipping over. Also note that, for simplicity, we decided to use only the axial forces F_z for mirror shape optimization. The lateral forces F_y are only used to support the mirror weight.

The details in deriving the horizon bending forces are found in Ref. [12]. We provide a

summary here.

- Ed Hileman provided a set of horizon forces, including F_z and F_y . The F_y forces, which are used to support the weight of the mirror at horizon pointing, came from some early Mirror Lab studies. They have a few discrete values, depending on the location and type of individual actuators. On the other hand, the F_z forces, although close to being optimized, still needed further optimization. Most likely Ed did the optimization early on using z -displacements. But these are just the starting point of our optimization. So it doesn't matter. We can converge to the optimal forces and surfaces with one correction.
- We applied the above forces in the latest M1M3 FEA model, at horizon pointing, and output the 3D displacements of each surface node.
- Surface normal displacements were calculated using the above 3D displacements.
- We optimized the surface shape using the surface normal displacements together with the FEA surface normal bending modes. This gives us a set of optimized F_z and the optimized surface shape it produces, when combined with the F_y which has been fixed.
- The above optimized forces were applied to the FEA model, so that we could output the 3D displacement vectors, calculate the surface normal shape, and compare to the optimized shape calculated above. This step is just a sanity check.
- Make a linear fit to the optimized F_z ,

$$F_z = by \quad (16)$$

Then subtract by from F_z

- Verify that the new F_z satisfies $\sum(F_z)=0$, $M_x=0$, and $M_y=0$.
- Determine the surface change that is produced by this force set using the FEA, i.e., determine zenith optimized forces and surface shape first, then add the balanced F_z forces from above, take the difference between the two set of 3D displacement vectors, convert to surface normal shape, and subtract PTT separately from M1 and M3. Alternatively, this step can be achieved outside of the FE model using the full influence matrix of the mirror.
- Based on the predicted force map and surface change, determine a scale factor to be used in Mirror Lab testing. (A surface RMS around 500nm is easiest to measure by the interferometers). The scale factor was determined to be 1/4.
- Apply the scaled forces in the Mirror Lab, make the M1-M3-M1 measurements before and after applying these additional forces. Take the difference, apply the invert of the scale factor, i.e., multiple by 4, compare to the FEA prediction.
- Fit the measured horizon bending shape to the FEA predicted shape. Obtain the scaling factor between measured and the FEA, and the residual map.

Figure 26 shows results from this test. The measured horizon bending shape and the FEA-predicted horizon bending shape are shown. After making the fit to the measured horizon shape using the FEA predicted shape, the scaling factor, which is the ratio between measured and FEA prediction, was found to be 1.039. Note that this shape is largely made of coma, i.e., bending mode No. 7. For earlier results, the scaling factor for bending mode No. 7 was found to be 1.032.

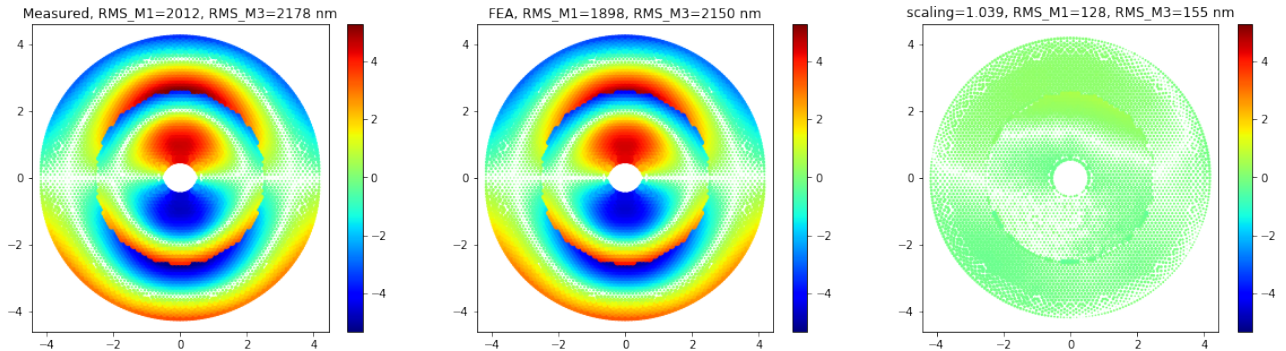


Figure 26: Results of horizon bending test. Left: measured horizon bending shape interpolated onto FEA grid, Center: FEA-predicted horizon bending shape, and Right: residual map from making a fit to the measured horizon shape using the FEA predicted shape. The scaling factor, which is the ratio between measured and FEA prediction, is found to be 1.039.

8.2 Inferring M1 shape from M3 measurements

For M1M3 horizon test on the summit, the plan has always been to test M3 only, because M1 radius of curvature will not be accessible. However, the horizon optimized forces F_{Gh} should optimize M1 and M3 surfaces simultaneously. So the question is, can we optimize M1 and M3 surfaces at the same time while we can only measure M3 shape? i.e., how well can we know M1 shape based on M3 measurements? As of the time this note is written, it looks unlikely that we will measure M3 interferometrically on the summit, due to potential challenges with interferometer alignment and amount of mechanical engineering work needed to put up the hardware. Instead, a Shack-Hartmann test for measuring M3 surface is being planned.

To answer the above question, the key is to realize that, what enables us to relate M1 surface with M3 surface is the fact that they are on one substrate, i.e., there is one set of forces. In the absense of measurement noise (on both the surface shape and the forces), any actuator under M1 can produce a noticeable shape change on M3, and vice versa. In that case, using M3 surface measurement, we can perfectly derive all the actuator forces. Multiplying that with the full mirror influence function gives of shapes of both M1 and M3.

But problems arise when there is noise. The forces for those actuators under M1 can be not accurately estimated using M3 surface measurement. The high spatial frequency components in the global M1M3 surface shape can not be inferred from M3 measurements alone. To suppress noise, we have to leave out the high frequency components on M3. The math, the results,

and the numerical analyses are documented in Document-32377 [13] and 32378 [14]. The basic conclusion was that inferring M1 shape from M3 measurements works for low order bending modes ($\sim < 15$), not high order one.

As documented in https://github.com/lsst-sitcom/M1M3_ML/blob/master/190221.ipynb, in the Mirror Lab, we started with 500nm of horizon deformation (about 1/4 of the inverse of the horizon gravitational sag), which is largely y-coma, and by keeping the first 15 singular values in the SVD the M3-only influence matrix, we reduced it by a factor of 3 (to 174nm) by optimizing M3 only. The 174nm comes from two sources.

1. One is that inferring M1 from M3 measurements simply does not work for the high order modes. Analysis shows that in the measured horizon test surfaces, the root-sum-square (RSS) of the high order modes (> 15) accounts for 148nm out of the 174nm of the total surface RMS. We know we cannot correct that. Modes 1-15 gives 481nm. $\sqrt{481^2 + 148^2} = 500$ nm. The high spatial order components are simply there, and we know we cannot do anything about it. So we choose to filter out the high order modes with data processing, specifically, when we try to infer all 156 forces using M3 measurements.
2. The other is the bending modes we use for this M1 prediction are FEA bending modes, which is different from the real mirror bending modes.

There are other sources as well, such as temperature drifts between the iterations, and measurement noise, which should be much smaller than 1 and 2 above. By filtering out the high order modes, we can largely avoid the amplification of the measurement noise, but there is no clean cut.

So if we do this on the summit, we will start from FEA predicted horizon forces. Without any axial force optimization we have 2 microns of surface deformation. If we assume 90% FEA accuracy, we will be off to ~ 200 nm. If we still reduce it by a factor of 3, we get to ~ 70 nm. We will not be able to reduce or eliminate item 2 above, because as we discussed in Section 7.3, we will use the bending mode shapes as they are derived from the FE analysis.

Since we only correct low order modes, we do not really need the high spatial resolution provided by the interferometer. In that sense, a SH would be good enough.

9 Actuator Force Error

Using the telemetry data collected during these tests, we have also been able to look at the difference between the applied forces and the measured forces. The applied forces are the forces as given by the force commands, found in the EFD table *m1m3_logevent_AppliedForces*. The measured forces are what the load cells tell us that has been applied, found in the EFD table *m1m3_ForceActuatorData*. The difference between the two reflects the ILC's ability to reach the target force values. For example, there may be a lack of air pressure, problems with the control valves, or just simply a glass safty limit.

In the analysis documented by https://github.com/lsst-sitcom/M1M3_ML/blob/master/ForceError.ipynb, we looked at actuator force differences within three 4-minute periods.

These were from three different days during test campaign No. 1. The three days are at the beginning, middle, and end of the test campaign. Ideally we would also pick some dates from test campaign No. 2. But problems with unintended data truncation in the EFD prevented us from doing that. More details are explained in the above notebook. We took three time stamps, each associated with some other measurements, as found in the per-day activities notebooks, and selected data within ± 2 minutes of those time stamps. The telemetry data was taken at frequency of 50 Hz. But there are some data missing in the EFD. So while taking the difference between the two sets of forces, we averaged each set of forces within 1-second time intervals. Another subtle thing here is that the database query has to be done using time stamps that the data was recorded in the EFD, which is in sequential order. When we match the two sets of forces, we had to use the time stamps when the telemetry messages were sent, which are not in sequential order sometimes, and therefore couldn't be used in the database query.

Figure 27 shows the force differences in their x, y, and z-components. Each entry in the histograms is a force difference for one actuator within a particular 1 second. The x and y force errors are basically negligible (compared to the force error requirement as shown in LTS-88 [15] Table 3). The z force errors can be as large as $2N$, which may require some attention. It is clear that the force error statistics is not drifting over time, i.e., this is repeatable over the entire period of test campaign No. 1.

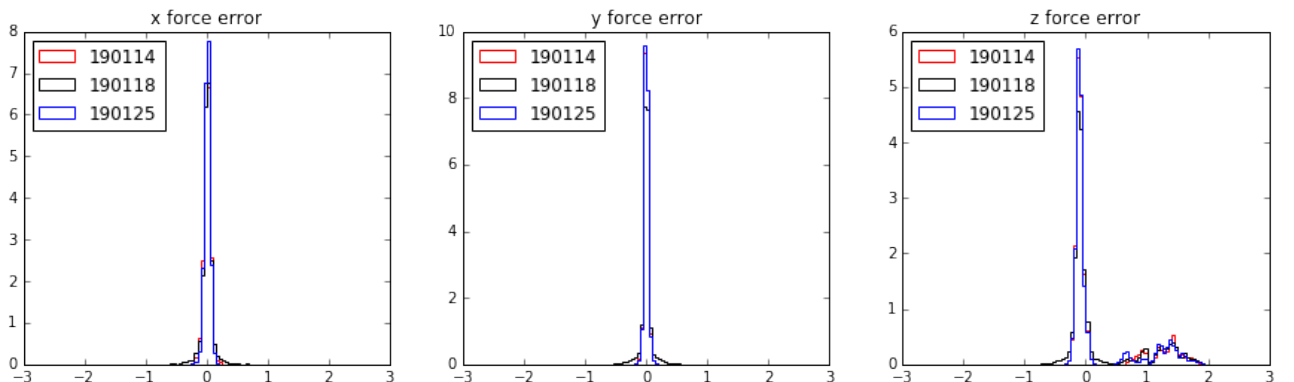


Figure 27: Actuator force error distributions within three 4-minute periods from different days during test campaign No. 1. For comparison purpose, each histogram is normalized to total area of 1.

Then the next question is, do the force errors vary by actuator? i.e., for a particular actuator, does it always have the same force error? To answer that question, we looked at the same kind of histograms, like those shown in Figure 27, by actuator. There are too many ($N=156$, for the z-forces) such histograms. We do not reproduce them here. Instead, the reader is referred to the notebook https://github.com/lsst-sitcom/M1M3_ML/blob/master/ForceError.ipynb. The conclusion there is that, indeed, the force errors for individual actuators are mostly repeatable. The non-repeatable errors, as shown by the width of the histograms, are negligible. LTS-88 [15] has the requirements on the non-repeating errors of the order $\sim 0.5N$. The repeatable force errors are as large as $\sim 2N$, but still well below those

required by LTS-88 [15] Table 3, which is 4.45N for x, y, and z forces.

We took the average of the per-actuator force error histograms, and produced a force offset table (found in the github repo, *data/* folder). We plan to add these systematic offsets to the control software, so that when force commands are sent out, these are already taken into account.

Note that this is separate from the calibration of the actuator load cells. If the load cells are not sufficiently calibrated, there could be errors and biases in the load cell reading. That could be an additional source of the force error. This calibration has been discussed in Section 7.2. The repeatable part of these force errors can also be easily taken out using the control software. Even if that is not done, they will largely be taken out by the AOS. It is the non-repeatable force error, which changes randomly with time, that could be more problematic. To the first order, they would produce nothing but astigmatisms on the mirror surfaces.

According to document-20263 [16], 0.5N non-repeating force errors produce about 5 mas of image degradation in effective FWHM. LTS-123 [17] and 124 [18] have the image quality allocation to M1M3 actuator force error as 10 mas. So we are well within the image quality budget here. Systematic calibration of all the load cells will allow us to further determine whether the contribution from actuator force errors is indeed below its image quality allocation.

10 Performance of the EFD

As we pointed out in Section 1, the performance of the EFD left a lot to be improved. While the EFD was supposed to capture all the telemetry, events, and commands as published by the M1M3 control software, the actual performance, as indicated by the capturing rate of the telemetry events, is shown in Figure 28. The absolute normalization of the y-axes is arbitrary due to histogram binning - each point covers 10 minutes time interval. In each case, the maximum of the y-ranges corresponds to telemetry capturing rate of 1. The M1M3 control system publishes telemetry at 50 Hz. The thermal data was published once a minute.

This version of the EFD, based on MariaDB, instead of the InfluxDB which will be used for final versions of the LSST EFD, worked $\sim 80\%$ of the time during campaign No. 1. During campaign No. 2 the capturing rate has been much worse, as seen in Figure 28. This is in addition to the force value truncation problem as we mentioned in Section 9.

11 Summary

Overall, the M1M3 optical testing at the UofA Mirror Lab has been a great success. We encountered some challenges along the way, mostly with surface optimization, but in the end we solved all the problems by understanding their causes, and we achieved the major goals of the testing campaigns. The only unachieved task as outlined in the test plan was to measure vibration when the cooling fans are turned on. This was not done due to problems turning on the cooling fans. But this was designed as an optional test from the very beginning.

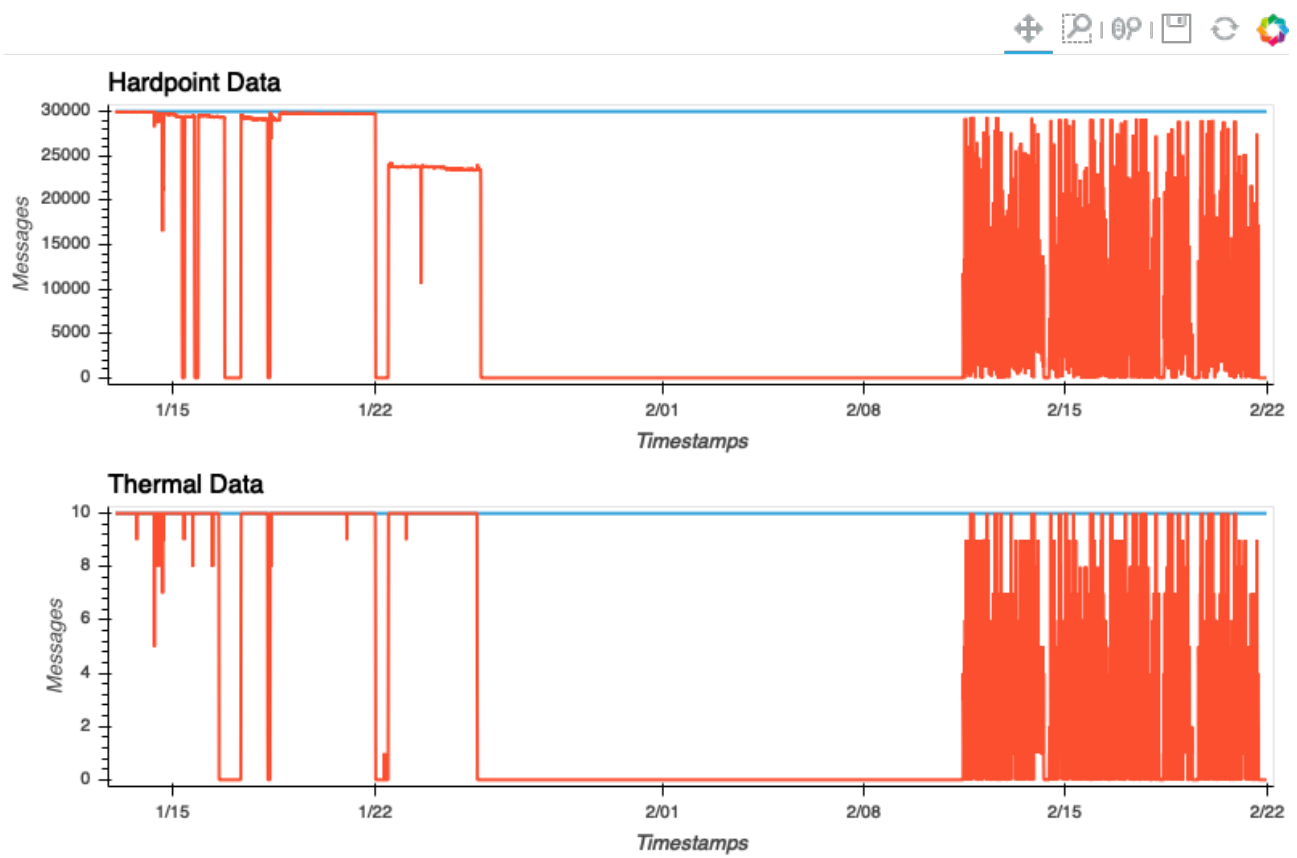


Figure 28: Some telemetry event rates as a function of time. The time range in these plots covers both test campaigns. Plots made by Michael Reuter.

These testing campaigns are the first step in building up our understanding of the entire LSST optical system. Once the system is reassembled in Chile, with the surrogate mirror instead of the real glass mirror, a portion of these tests will be repeated on the summit. After we do the M3 testing on the summit, we will update the LUT by replacing the horizon FEA-determined optimal forces with the measured optimal forces. Then the M1M3 LUT will be ready to go on sky with the three-mirror system.

References

- [1] B. Xin, G. Angeli, and C. Claver, “Optical Performance of LSST Primary-Tertiary Mirror,” *LSST Docushare Document-17171*, 2015.
- [2] The Richard F. Caris Mirror Lab and the LSST M1M3 team, “M1M3 Testing in Telescope Cell – Test Plan Execution,” *LSST Docushare Document-34904*, 2019.
- [3] B. Xin, “Data analysis plan presented at M1M3 Optical Test Readiness Review,” *LSST Docushare Document-34905*, 2015.
- [4] B. Xin et. al., “M1M3 Data Reduction Pipeline,” *LSST Docushare Document-17912*, 2015.
- [5] The Richard F. Caris Mirror Lab, “LSST M1/M3 Test in Operational Support Cell Data Analysis Report,” *LSST Docushare Document-34910*, 2019.
- [6] G. Angeli, “M1M3 Substrate Bending Modes,” *LSST Docushare Document-15312*, 2013.
- [7] B. Xin, “M1M3 Surface Sag and Surface Normal,” *LSST Docushare Document-16390*, 2014.
- [8] B. Xin, E. Hileman, and D. Neil, “Initial Actuator Support Forces for M1M3 Optical Testing,” *LSST Docushare Document-32192*, 2019.
- [9] E. Hileman, “FEA investigation of divits above the quads,” *LSST Docushare Document-34906*, 2019.
- [10] B. Xin, “Do we need bending mode 27 for AOS closed-loop?,” *LSST Docushare Document-34909*, 2019.
- [11] B. Xin, “M1M3 and M2 Force Budgets As Inputs to AOS Control,” *LSST Docushare Document-34826*, 2018.
- [12] B. Xin, “M1M3 Horizon Test Force Determination,” *LSST Docushare Document-31103*, 2018.
- [13] B. Xin, “Infer M1 surface from M3 measurement - part I,” *LSST Docushare Document-32377*, 2018.
- [14] B. Xin, “Infer M1 surface from M3 measurement - part II,” *LSST Docushare Document-32378*, 2018.
- [15] J. Sebag, D. Neil, C. Araujo, and A. Serio, “M1M3 Mirror Support Design Requirements Document,” *LSST Docushare LTS-88*, 2017.

- [16] B. Xin, “M1M3 actuator force accuracy requirement study,” *LSST Docushare Document-20263*, 2015.
- [17] J. Sebag, “Telescope Error Budget,” *LSST Docushare LTS-123*, 2011.
- [18] J. Sebag, “Telescope Error Budget,” *LSST Docushare LTS-124*, 2011.